Temporal overlap of excitatory and inhibitory afferent input in guinea-pig CA1 pyramidal cells

Sergei Karnup and Armin Stelzer

Department of Physiology and Pharmacology, State University of New York, Health Science Center at Brooklyn, Brooklyn, NY 11203, USA

(Received 13 July 1998; accepted after revision 11 January 1999)

1. The temporal interaction of evoked synaptic excitation and $GABA_A$-mediated inhibition was examined in CA1 pyramidal cells. Single and paired intracellular recordings were carried out in pyramidal cell dendrites and somata, and interneurons of the guinea-pig hippocampal slice. Current-clamp, sharp electrode and whole-cell voltage-clamp recordings were made.

2. Kinetics of dendritic and somatic inhibitory responses were similar. Notably, kinetics of dendritic unitary IPSPs were as fast as kinetics of somatic unitary IPSPs.

3. $GABA_A$-mediated influences were present throughout the orthodromic pyramidal cell EPSP/EPSC. Comparison of the kinetics of pharmacologically isolated monosynaptic IPSPs, IPSCs and inhibitory conductances (g_{GABA_A}), showed fastest kinetics for g_{GABA_A}. Close temporal overlap was observed between monosynaptic g_{GABA_A} and the rising phase of the evoked EPSP/EPSC. The onset of g_{GABA_A} coincided with or preceded onset of the EPSP/EPSC.

4. Onsets of feedforward IPSPs coincided with the rising phase of the pyramidal cell EPSP in $> 80\,\%$ of paired recordings. Fastest feedforward inhibitory responses exerted near complete overlap with evoked excitation.

5. Onsets of recurrent IPSPs did not occur during the rising phase of the evoked EPSP, but $> 3{\cdot}0$ ms after the peak of the pyramidal cell EPSP.

6. Orthodromically evoked interneuron spikes were observed at stimulation intensities that were below the threshold for eliciting EPSPs in concomitantly recorded pyramidal cells. The activation of feedforward inhibitory responses by weakest excitatory input, and the large temporal overlap between feedforward inhibition and evoked excitation, suggest that *in situ* any excitatory input in CA1 is effectively controlled by fast synaptic inhibition.

The response to afferent fibre stimulation ('orthodromic response') is a commonly used measure of excitability of neuronal populations. An excitatory (EPSP) and inhibitory (IPSP) component was identified by studies of the orthodromic response in hippocampal pyramidal cells *in vivo* (Kandel *et al.* 1961; Andersen *et al.* 1963, 1964). This basic sequence of orthodromic EPSP–IPSP has been confirmed since then: the response that is elicited by stimulation of the Schaffer collateral–commissural pathway consists of a fast EPSP/EPSC mediated primarily by AMPA receptors, followed by an early IPSP/IPSC mediated by $GABA_A$ receptors and a late IPSP/IPSC mediated by $GABA_B$ receptors. Despite such clear separation of postsynaptic potentials (PSPs) or currents (PSCs), it is conceivable that inhibitory influences may be present long before the population IPSP is expressed. If so, how large is the temporal overlap with the orthodromic EPSP/EPSC?

This study has focused on three points. First, the kinetics of dendritic inhibition were studied. Several previous studies have reported that the kinetics of dendritic inhibitory responses were slower than those of somatic responses in pyramidal cells (Miles, 1990*b*; Pearce, 1993; Buhl *et al.* 1994*a*). Second, kinetics of different inhibitory responses, i.e. IPSPs, IPSCs and conductance changes, were investigated. It was suggested that inhibitory conductance changes are faster than IPSPs (Araki *et al.* 1960) or inhibitory currents (Koch, 1985). Third, time courses of various components of the circuitry were studied: a monosynaptic inhibitory response is elicited via direct electrical stimulation of interneuron processes (Davies *et al.* 1990). Activation of afferent fibres results in a feedforward inhibitory response in CA1 pyramidal cells via synaptic activation of CA1 interneurons (Knowles & Schwartzkroin, 1981; Alger & Nicoll, 1982; Buzsaki & Eidelberg, 1982; Ashwood *et al.*

1984; Lacaille & Schwartzkroin, 1988; Lacaille, 1991; Buhl *et al.* 1994*b*). A recurrent inhibitory response is activated by synaptic pyramidal cell action potentials (APs) (Kandel *et al.* 1961; Andersen *et al.* 1963, 1964).

Knowledge of the temporal interaction between inhibitory components and orthodromic excitation is pivotal for the understanding of how activity-dependent changes of inhibition will affect the orthodromic EPSP. Activity-dependent impairment of $GABA_A$ receptor function (Stelzer *et al.* 1994; Wang & Stelzer, 1996) decreases the efficacy of all three inhibitory components. Possible increase of interneuron excitability (interneuron long-term potentiation; Buzsaki & Eidelberg, 1982; Taube & Schwartzkroin, 1987; Stelzer *et al.* 1994; Quardouz & Lacaille, 1995) will enhance the efficacy of feedforward inhibition. The efficacy of recurrent inhibition is enhanced by both pyramidal cell long-term potentiation (LTP) and interneuron LTP.

METHODS

Brain slices

Transverse hippocampal slices (Yamamoto, 1972; Schwartzkroin, 1975) were obtained from adult guinea-pigs (Hartley, from Harlan Sprague–Dawley, Inc., Indianapolis, IN, USA; 150–200 g). Guinea-pigs were anaesthetized by inhalation of halothane (2-bromo-2-chloro-1,1,1-trifluoroethane) before decapitation with an animal guillotine. After removal of the brain and isolation of the hippocampus, slices of 450 μm thickness were cut on a McIlwain tissue chopper. The procedures conformed with the guidelines of the Institutional Animal Care and Use Committee (protocol no. 9808069). Slices were superfused in an interface recording chamber (Fine Science Tools, Belmont, CA, USA) with a solution saturated with 95% O_2 and 5% CO_2 (temperature, 30–32 °C) of the following composition (mM): 118 NaCl, 3 KCl, 25 $NaHCO_3$, 1·2 NaH_2PO_4, 1·2 $MgCl_2$, 1·7 $CaCl_2$ and 11 D-glucose.

Electrophysiological recordings

Sharp electrode recordings. Sharp microelectrode recordings in current clamp or discontinuous single-electrode voltage clamp (dSEVC) were carried out in CA1 pyramidal cells ($n = 43$ in somata, $n = 62$ in apical dendrites) and stratum pyramidale interneurons ($n = 29$). Impalements were made with glass pipettes (World Precision Instruments, Inc., Sarasota, FL, USA) pulled using a Brown–Flaming electrode puller (Model P-87, Sutter Instrument Co., Novato, CA, USA). Tracking was performed with manually controlled manipulators (Narishige, Tokyo, Japan). The standard electrode content of pyramidal cell recordings was potassium acetate (2–3 M) yielding 40–100 MΩ electrode resistances. Identification criteria for dendritic recordings were the recording site in stratum radiatum (between 150 and 400 μm perpendicular to stratum pyramidale) and burst responses to current injection (Wong *et al.* 1979).

Interneuron identification. Interneurons were recorded singly or simultaneously with pyramidal cells. The following criteria were used to identify interneurons physiologically (Schwartzkroin & Mathers, 1978): symmetrical spike shape (Fig. 5*A*, inset), prominent spike afterhyperpolarization (AHP; Fig. 5*B*, inset) and firing patterns (e.g. Fig. 5*B*, inset). Intracellular biocytin staining (2% in 2 M potassium acetate; see Somogyi & Takagi, 1982; Buhl *et al.* 1994*a*) was used to distinguish three subtypes of CA1 stratum pyramidale interneurons based on their axonal arborization (Fig. 5*E*) (Buhl *et al.* 1994*a*; Miles *et al.* 1996). Stained cells were viewed in a Nikon Optiphot-2 microscope. Twenty-eight of 97 physiologically identified interneurons could be held long enough for sufficient biocytin filling and conclusive subtype identification (see Table 3).

For dual interneuron–pyramidal cell recordings, the interneuron recording was always established first. Only interneurons that exhibited no spontaneous firing at resting membrane potential were studied; spontaneously firing cells were discarded. A concomitant dendritic pyramidal cell recording – without biocytin in the recording pipette – was then established in stratum radiatum (within 100–400 μm from the interneuron location). Synaptic coupling between the two neurons was tested by eliciting APs in the interneuron (through injection of depolarizing current pulses, 0·1–0·6 nA, 200–300 ms duration). If a monosynaptic IPSP in response to interneuron AP could not be established, the dendritic recording was usually discontinued after a few orthodromic responses. Additional dendritic (up to eight in two pairs) and then somatic pyramidal cell recordings were carried out as long as the interneuron lasted.

Whole-cell voltage-clamp recordings. Whole-cell voltage-clamp recordings were performed in pyramidal cell somata using the 'blind' tracking method (Blanton *et al.* 1989; Marty & Neher, 1995). Patch pipettes were pulled from thin-walled borosilicate glass without filaments (1·5 mm o.d., 1·17 mm i.d.; TW 150-6, from WPI) on a Brown–Flaming puller (Sutter Instruments). Tip diameters (1 μm), which were routinely assessed under the light microscope, yielded electrode resistances between 3 and 6 MΩ. For seal formation, the amplifier (Axoclamp-2A, Axon Instruments, Inc., Foster City, CA, USA) was set to continuous ('bridge') mode and current pulses (0·1–0·2 nA, 20 ms, repeated every 100 ms) were injected. Patch electrode settling and capacitance compensation were performed in current clamp. Electrode time constants were shortened with capacitance compensation to 10–30 μs. Sampling frequencies were 5–7 kHz.

Data aquisition and analysis

Evoked responses were elicited by stimulation of stratum radiatum Schaffer collateral–commissural fibres through a pair of insulated tungsten bipolar electrodes (stimulation range 15–800 μA). Voltage signals of dual recordings were recorded and amplified with an Axoprobe-1A (Axon Instruments). Voltage and current signals of single recordings recorded in both dSEVC and current clamp were amplified by Axoclamp (Axon Instriments). Data were sampled at rates ranging from 2·5 to 10 kHz (−3 dB) and filtered with a cut-off frequency of 1·5 kHz. The voltage and current signals were fed into separate channels of an A/D converter (Digidata 1200, Axon Instruments) digitized, stored and analysed off-line using pCLAMP6 software from Axon Instruments on a Pentium PC. Statistical significance was accepted at the $P < 0{\cdot}05$ level in various tests.

Drugs

With the exception of intracellularly applied biocytin (Sigma), all drugs, bicuculline (Bic), picrotoxin (PTX), 6-cyano-7-nitro-quinoxaline-2,3-dione (CNQX), D-aminophosphonovalerate (D-AP5) and saclofen, were applied by bath perfusion. CNQX, D-AP5 and saclofen were purchased from Tocris Cookson, Inc. (Ballwin, MO, USA); all other drugs were from Sigma.

Abbreviations

$t_{(i)}$ is the poststimulation latency to the event specified by the subscript. For example, $t_{(\mathrm{P,mono\ IPSP,onset})}$ denotes the latency between stimulation artifact and onset of the stimulation-evoked monosynaptic IPSP in a pyramidal (P) cell.

$\Delta t_{(i-j)}$ is the time lag between two events. For example, $\Delta t_{(\mathrm{I,AP,peak-P,IPSP,onset})}$ denotes the latency between peak of an AP in an interneuron (I) and onset of the unitary IPSP in a synaptically coupled pyramidal cell.

$g_{\mathrm{GABA_A}}$ is the $\mathrm{GABA_A}$ receptor-mediated conductance. AHP denotes afterhyperpolarization; V_{m} is membrane potential, V_{thres} is AP threshold potential, and V_{rest} is resting membrane potential.

RESULTS

The aim of this study was to evaluate the temporal overlap between the excitatory and inhibitory components of the orthodromic response in CA1 pyramidal cells. At what poststimulation latency of the orthodromic response are $\mathrm{GABA_A}$-mediated influences present? The large enhancement of all non-$\mathrm{GABA_A}$ components of the orthodromic response (EPSP and late IPSP, respectively) during PTX application (Fig. 1*A*) indicates that $\mathrm{GABA_A}$-mediated influences are present throughout the orthodromic response. Notably, enhancement of the EPSP slope by $\mathrm{GABA_A}$ antagonists (Fig. 1*Aa* and *B*) suggests that fast synaptic inhibition controls the rising phase of the orthodromic EPSP: in six dendritic pyramidal cell recordings, bicuculline (100 μM) application increased EPSP slopes between 167 and 1048% (mean, 372 ± 69%). D-AP5 (40–100 μM) was present throughout the experiments (see Fig. 1*B*), which demonstrates that the EPSP increase was not caused by NMDA-dependent potentiation of AMPA currents (cf. Pananceau *et al.* 1997). In about a third of dendritic recordings, a small IPSP preceded the onset of the orthodromic EPSP (Fig. 1*B*).

Monosynaptic inhibition

Comparison of the kinetics of orthodromic excitation and monosynaptic inhibition in the same cells was achieved by the following protocol: the orthodromic response was recorded first. The same stimulation (with respect to site and intensity) was then applied following application of CNQX, D-AP5 and saclofen (Figs 2–4; Table 1). The resulting pharmacologically isolated inhibitory responses (monosynaptic IPSP, IPSC and conductance change ($g_{\mathrm{GABA_A}}$)) were in all cases completely blocked by bicuculline (100 μM, not shown).

Temporal comparison of monosynaptic IPSP/IPSC and EPSP/EPSC. In nine dendritic and seven somatic preparations, recordings were carried out in both current clamp and dSEVC (Figs 2–4; Table 1A).

Kinetics of IPSCs were faster than IPSPs (Table 1A; Fig. 2*D*). Mean differences between $t_{(\mathrm{IPSP,peak})}$ and $t_{(\mathrm{IPSC,peak})}$ were 5·7 ± 0·7 ms in dendritic ($n = 9$) and 5·2 ± 0·5 ms in somatic ($n = 7$) recordings. In contrast to IPSP/IPSCs, no significant differences in kinetics were observed between EPSPs and EPSCs: mean differences between $t_{(\mathrm{EPSP,peak})}$ and $t_{(\mathrm{EPSC,peak})}$ were only 0·8 ± 0·2 ms in dendritic ($n = 9$) and 0·7 ± 0·3 ms in somatic ($n = 7$) recordings.

The latencies to onsets of all responses – orthodromic EPSP/EPSCs, monosynaptic IPSP/IPSCs – were statistically identical in both groups of recordings, somata and dendrites (ANOVA) (Table 1A). With the exception of latencies to onset, however, kinetics of IPSP/IPSCs were considerably slower than those of EPSP/EPSCs. For example, rise times (10–90%) and latencies to peak of the monosynaptic IPSP, were on average more than twice as long as those of the orthodromic EPSP (Table 1A and B, Fig. 2*B*). Mean differences between $t_{(\mathrm{EPSP,peak})}$ and $t_{(\mathrm{IPSP,peak})}$ were 8·0 ± 1·1 ms in dendritic and 10·6 ± 1·6 ms in somatic recordings. Temporal overlap between EPSP and IPSP was modest (Fig. 2*B*). Due to the faster kinetics of IPSCs, mean

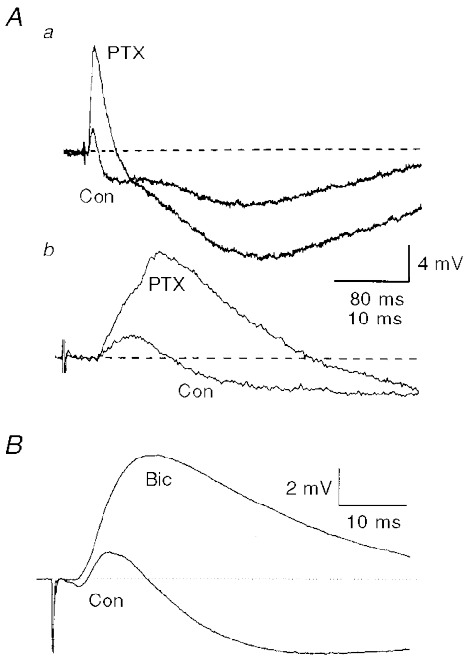

Figure 1. Effects of $\mathrm{GABA_A}$ receptor blockade on orthodromic potentials in CA1 pyramidal cells

Aa, superimposed responses in a pyramidal cell soma before and after application of picrotoxin (PTX, 100 μM). Control and PTX recordings were obtained at V_{rest} (−64 mV; 150 μA stimulation intensities; 1000 μm distance between stratum radiatum stimulation site and perpendicular line through stratum pyramidale recording site). *Ab*, depiction of same recordings (shown above) on an extended time scale. *B*, superimposed orthodromic responses in a CA1 pyramidal cell apical dendrite before (Con) and after application of bicuculline (Bic, 100 μM). Bicuculline was added to D-AP5 (40 μM)- and saclofen (100 μM)-containing control solution. Each trace (Con and Bic) represents the average of 15 individual recordings. Recordings were obtained at V_{rest} (−63 mV) by the same stimulation protocol (65 μA, 100 μs). All recordings in *A* and *B* were carried out in 'minislices' in which the CA3 region was cut off by dissection.

Table 1. Kinetics of stimulation-evoked excitatory (EPSP, EPSC) and monosynaptic inhibitory responses (IPSP, IPSC, g_{GABA_A})

A. PSP/Cs	Dendrites ($n = 9$)	Somata ($n = 7$)
$t_{(EPSP,onset)}$ (ms)	2·8 ± 0·5	2·9 ± 0·5
$t_{(IPSP,onset)}$ (ms)	2·8 ± 0·3	2·8 ± 0·6
$t_{(EPSC,onset)}$ (ms)	2·7 ± 0·3	3·0 ± 0·5
$t_{(IPSC,onset)}$ (ms)	3·1 ± 0·7	3·0 ± 0·3
$t_{(EPSP,peak)}$ (ms)	7·7 ± 0·5	7·6 ± 0·7
$t_{(IPSP,peak)}$ (ms)	16·7 ± 1·3 *	18·1 ± 1·9 *
$t_{(EPSC,peak)}$ (ms)	7·0 ± 0·6	7·1 ± 0·6
$t_{(IPSC,peak)}$ (ms)	11·2 ± 2·1 *†	13·3 ± 1·7 *†
B. PSPs and g_{GABA_A}	**Dendrites ($n = 14$)**	**Somata ($n = 11$)**
g_{GABA_A}, rise time (ms)	2·7 ± 0·4	2·9 ± 0·6
IPSP, rise time (ms)	5·7 ± 1·1 *	6·6 ± 0·8 *
EPSP, rise time (ms)	2·6 ± 0·5	2·7 ± 0·6
$t_{(peak,g_{GABA,A})}$ (ms)	6·1 ± 0·7	6·9 ± 0·9
$t_{(IPSP,peak)}$ (ms)	15·2 ± 2·1 *	18·3 ± 2·4 *
$t_{(EPSP,peak)}$ (ms)	7·0 ± 0·6	6·8 ± 0·8
$t_{(AP,peak)}$ (ms)	7·1 ± 1·4 ($n = 3$)	7·0 ± 1·1 ($n = 4$)
C. g_{GABA_A} (% of peak)	**Dendrites ($n = 14$)**	**Somata ($n = 11$)**
Percentage of peak at $t_{(IPSP,onset)}$	15·8 ± 3·6	11·1 ± 2·3
Percentage of peak at $t_{(IPSP,peak)}$	75·5 ± 8·4	70·5 ± 10·9
Percentage of peak at $t_{(EPSP,onset)}$	13·8 ± 4·6	10·7 ± 3·7
Percentage of peak at $t_{(EPSP,peak)}$	94·1 ± 5·5	91·9 ± 7·3
Percentage of peak at $t_{(AP,onset)}$	94·5 ± 7·4 ($n = 3$)	93·2 ± 9·4 ($n = 4$)
D. PSP/Cs and g_{GABA_A}	**Dendrites ($n = 7$)**	**Somata ($n = 4$)**
$t_{(IPSP,peak)}$ (ms)	18·4 ± 3·6	20·4 ± 4·2
$t_{(IPSC,peak)}$ (ms)	12·3 ± 2·3 *	13·9 ± 3·3 *
$t_{(peak,g_{GABA,A})}$ (ms)	6·5 ± 0·9 *	7·1 ± 2·1 *
$t_{(EPSP,peak)}$ (ms)	6·1 ± 1·0	6·7 ± 1·5
$t_{(EPSC,peak)}$ (ms)	6·2 ± 0·8	6·5 ± 1·2

A, kinetics of stimulation-evoked EPSPs, EPSCs, IPSPs and IPSCs recorded alternately in current-clamp and voltage-clamp mode in the same cells. In all comparisons, values of latencies to onset (EPSP, EPSC, IPSP, IPSC) were statistically identical in dendritic and somatic recordings ($P > 0·05$, ANOVA). B and C, kinetics of inhibitory conductances (g_{GABA_A}), EPSP and IPSP. B, comparison of rise time and latencies to peaks; C, percentage of the peak value of g_{GABA_A} at the time of denoted parameters. Peak g_{GABA_A} were 13·5 ± 4·6 nS (mean ± S.E.M. in 14 dendritic recordings) and 11·3 ± 3·6 nS (11 somatic recordings). D, latencies to peaks of g_{GABA_A}, IPSC, IPSP, EPSP and EPSC recorded in current clamp and discontinuous single-electrode voltage clamp in the same cells. In all recordings, respective orthodromic excitatory responses (EPSPs, EPSCs) were recorded first, respective inhibitory responses (IPSPs, IPSCs, g_{GABA_A}) following application of CNQX (20–100 μM), D-AP5 (40–100 μM) and saclofen (100 μM). The stimulation protocol (intensity adjusted to generate half-maximal EPSPs; 500 μm distance between recording and stimulation sites) was applied to elicit EPSP/EPSCs and IPSP/IPSCs, g_{GABA_A}. Data are depicted as means ± S.E.M. separated into recordings of somata and apical dendrites of CA1 pyramidal cells (n = number of recordings). t denotes the time of poststimulation latency measured from the onset of the stimulation artifact (see Fig. 2*B*). In all comparisons (A–D), kinetics of the same parameter showed no significant differences between dendritic and somatic recordings. * Significant difference between the inhibitory and excitatory parameter listed in the row above (e.g. $t_{(IPSP,peak)}$ and $t_{(EPSP,peak)}$); † significant difference between $t_{(IPSC,peak)}$ and $t_{(IPSP,peak)}$.

differences between $t_{(EPSC,peak)}$ and $t_{(IPSC,peak)}$ were somewhat smaller: 4·3 ± 0·7 ms in dendritic ($n = 9$) and 7·1 ± 0·9 ms in somatic recordings ($n = 7$). However, temporal overlap between EPSC and IPSC was still rather small (Fig. 2*C*). The same conclusion was reached when comparing EPSCs and IPSCs that were measured in somatic whole-cell recordings. Latencies to $t_{(EPSC,peak)}$ (5·8 ± 1·2 ms; $n = 5$) and to $t_{(IPSC,peak)}$ (12·5 ± 1·5 ms; $n = 5$) and mean differences (6·8 ± 1·2 ms) were not statistically different when comparing the respective values obtained from sharp-electrode and whole-cell recordings ($P > 0·05$, ANOVA).

Kinetics of $GABA_A$-mediated conductances (g_{GABA_A}). Inhibitory conductance changes (g_{GABA_A}) were obtained by the membrane voltage deflection in response to short hyperpolarizing current pulses during the monosynaptic inhibitory response (Fig. 3*A*). In 14 dendritic and 11 somatic recordings, both g_{GABA_A} and corresponding IPSPs were measured (Table 1B and Fig. 3*C*). The comparison demonstrated considerably faster kinetics of conductances. Rise times (10–90 %) of g_{GABA_A} were on average > 2 times faster than those of IPSPs (Table 1B). Poststimulation latencies to peak of g_{GABA_A} ($t_{(peak\ g_{GABA,A})}$) were about 2·5 times faster than latencies to IPSP peak in the same recordings (Table 1B). Similar to inhibitory conductance changes in motoneurons (Araki *et al.* 1960), peak values of g_{GABA_A} coincided with the rising phase of the monosynaptic IPSP (Fig. 3*C*). In addition, net expression of g_{GABA_A} was observed at $t_{(IPSP,onset)}$ in 7 of 11 somatic and 12 of 14 dendritic recordings (Table 1B; Fig. 3*B* and *C*). At $t_{(IPSP,onset)}$, g_{GABA_A} was expressed between 10–15 % of maximal values.

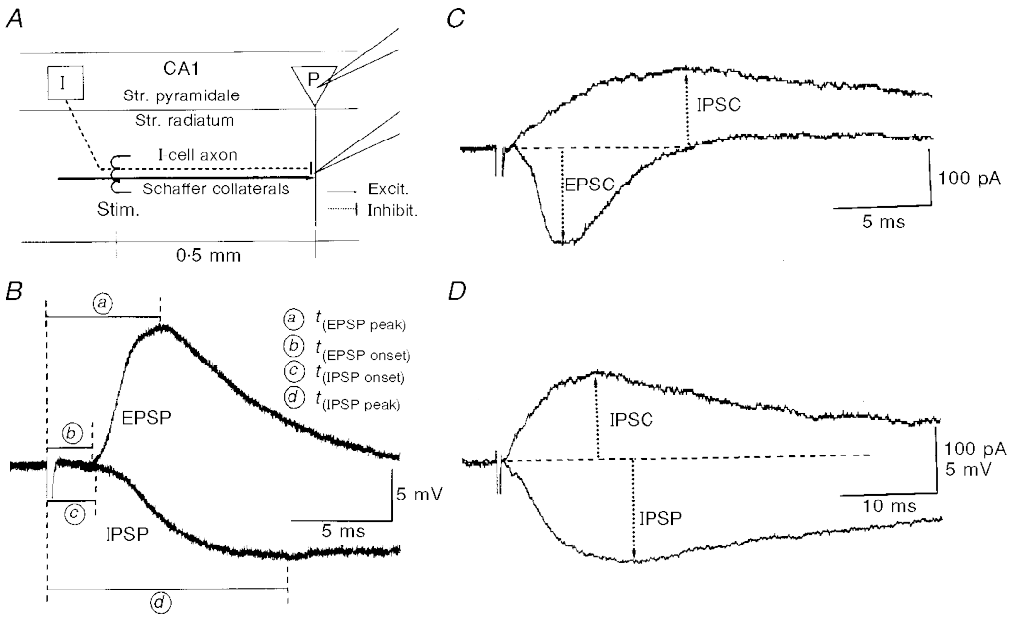

Figure 2. Comparison of time courses of stimulation-evoked monosynaptic EPSP/EPSCs and IPSP/IPSCs

A, schematic depiction of the CA1 circuitry and experimental protocol. Stratum (Str.) radiatum stimulation produced an initial monosynaptic EPSP/EPSC (*B* and *C*) through excitatory afferents (Schaffer collaterals). Block of synaptic excitation and $GABA_B$-mediated inhibition revealed a monosynaptic $GABA_A$ receptor-mediated IPSP/IPSC (Davies *et al.* 1990) (*B* and *D*) via direct stimulation of interneuron cell processes (dashed line, I-cell axon; see Fig. 5). *B*, superimposed recordings of stimulation-evoked EPSP and monosynaptic IPSP following application of CNQX (40 μM), D-AP5 (50 μM) and saclofen (100 μM). Recordings were obtained in the same CA1 pyramidal cell apical dendrite (150 μm from stratum pyramidale) at different V_m: EPSP at −79 mV, IPSP at −64 mV (i.e. V_{rest}). The distance between stratum radiatum stimulation and dendritic recording site was about 0·5 mm. Poststimulation latencies were measured from the onset of the stimulation artifact. Values calculated for this recording were: EPSP peak ($t_{(EPSP,peak)}$, *a*), 5·8 ms; EPSP onset ($t_{(EPSP,onset)}$, *b*), 2·3 ms; IPSP onset ($t_{(IPSP,onset)}$, *c*), 2·5 ms; IPSP peak ($t_{(IPSP\ peak)}$, *d*), 12·4 ms. EPSP slope (10–90 %) was 5·83 mV ms^{-1}, IPSP slope during the same poststimulation latencies was 1·22 mV ms^{-1}. *C*, superimposed EPSC and IPSC (in dSEVC, sampling rate: 4·8 kHz). EPSC was recorded under control conditions near the chloride reversal potential (−79 mV). The IPSC was recorded after pharmacological isolation of $GABA_A$ response at V_{rest} −64 mV. The EPSC slope (10–90 %) was 47·34 pA ms^{-1}; IPSC slope in the same time range was 12·11 pA ms^{-1}. *D*, superimposed recordings of stimulation-evoked IPSC and IPSP. Latency to IPSC peak was 9·8 ms. All recordings were obtained in the same cell by the same stimulation protocol (120 μA intensity, 80 μs duration), which was chosen during control to generate about 50 % of the subthreshold EPSP amplitude.

Inhibitory conductances also exhibited faster kinetics than IPSCs; experiments in which all parameters, EPSP/EPSC, IPSP/IPSC and g_{GABA_A}, were measured in a given cell (7 dendrites, 4 somata: e.g. cell shown in Figs 2–4) confirmed a distinct order of 'speed' (Table 1D): g_{GABA_A} > IPSC > IPSP. For example, in the seven dendritic recordings in which all three inhibitory parameters (IPSP, IPSC, g_{GABA_A}) were measured, average poststimulation latencies to peaks were 6·5 ms (g_{GABA_A}), 12·3 ms (IPSC) and 18·4 ms (IPSP). Similar differences were observed in somatic recordings (Table 1D).

Temporal comparison of EPSP/EPSCs and g_{GABA_A}. Close temporal correlation was observed between the rising phases of g_{GABA_A} and orthodromic excitation (Fig. 4*A–C*): comparing EPSP and g_{GABA_A}, both the rise times (10–90 %) and latencies to peak were statistically not different in dendritic and somatic recordings (Table 1B). At $t_{(EPSP,peak)}$, g_{GABA_A} were > 90 % of their respective peak values in all recordings. The best correlation ($r = 0{\cdot}941$) was observed between $t_{(EPSC,peak)}$ and $g_{(peak,GABA_A)}$ in dendritic recordings.

Onset of g_{GABA_A} preceded onset of EPSP in 13 of 14 dendritic and 8 of 11 somatic recordings. At EPSP onset,

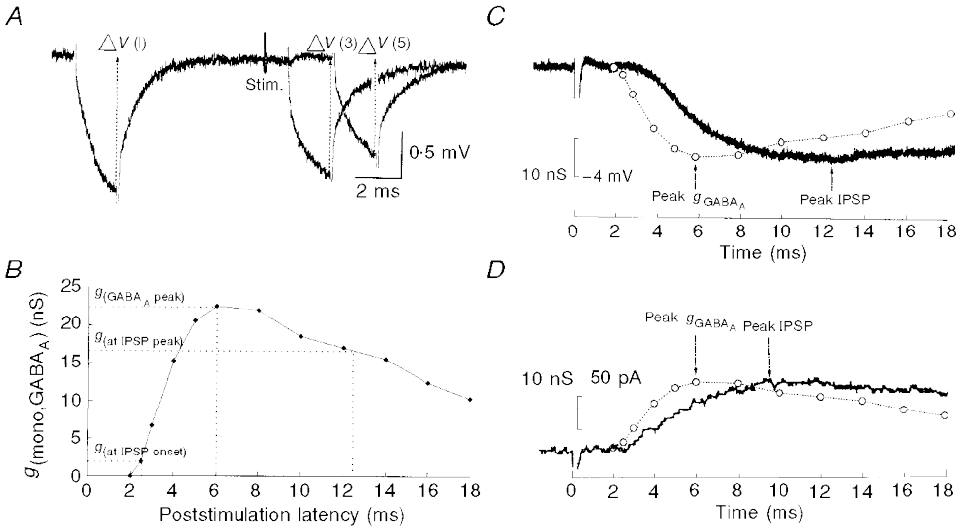

Figure 3. Membrane conductance increases during the monosynaptic inhibitory response (g_{GABA_A})

A, experimental protocol of measuring g_{GABA_A}. Recordings were carried out in the presence of CNQX (40 μM), D-AP5 (50 μM) and saclofen (100 μM) in CA1 pyramidal cell apical dendrite at V_{rest} (−64 mV). Two hyperpolarizing current pulses (each 2 ms duration, −0·6 nA) were applied, one before electrical stimulation, the second at various points of time following stimulation. Membrane voltage deflections in response to current injection were isolated from the underlying IPSP by subtracting a second response in which the IPSP was elicited without concomitant current pulses (Stelzer *et al.* 1994). The voltage deflection in response to the pulse before electrical stimulation ('ΔV(l)') was used for the assessment of leak conductance, the voltage deflection caused by the second pulse for assessment of net conductance increase during the inhibitory response. Depicted are two superimposed traces with poststimulation pulses applied at $t = 3$ and $t = 5$ ms, respectively. Values of g_{GABA_A} (as shown in *B*) were calculated based on the voltage deflections measured at the end of the 2 ms current pulse: the voltage deflection at $t = 3$ ms ($\Delta V(3)$) was used for calculation of g_{GABA_A} at $t = 3$ ms; $\Delta V(5)$ was used for calculation of g_{GABA_A} at $t = 5$ ms. Reliable measurements of $\Delta V(t)$ by 2 ms pulses required careful bridge balancing and capacitance neutralization. During the rising phase of g_{GABA_A} ($t = 2$ to $t = 6$ ms), measurements and calculations were carried out at 1 ms intervals, whereas 2 ms intervals were applied from $t = 6$ to $t = 20$ ms. g_{GABA_A} was calculated by the following formula: $g_{GABA_A} = (i(1 - \exp(-t_p/\tau_m))/\Delta V(t)) - g_{leak}$, with $g_{leak} = i(1 - \exp(-t_p/\tau_m))/\Delta V_{leak}$; g_{leak} is leak conductance; i is (hyperpolarizing) current injected during the 2 ms pulse (in the cell depicted, −0·6 nA); t_p is duration of current pulse; and τ_m is membrane time constant (here 20 ms; assessed by 300 ms hyperpolarizing current pulse, not shown). *B*, graph of g_{GABA_A} as a function of poststimulation latency for the recording shown in Figs 2 and 3*A*. The value of peak conductance ($g_{(GABA_A,peak)}$) was defined as maximal value of all measurements (in the recording depicted, 22·5 nS at $t = 6$ ms). GABA conductances at $t_{(IPSP,onset)}$ and $t_{(IPSP,peak)}$ were determined by extrapolation from the curve of g_{GABA_A} at the respective latencies $t_{(IPSP,onset)} = 2{\cdot}5$ ms and $t_{(IPSP,peak)} = 12{\cdot}4$ ms. In the depicted recording, $g_{(IPSP,onset)}$ was 1·9 nS, which was 8·4 % of $g_{(GABA_A,peak)}$, and $g_{(IPSP,peak)}$ was 16·6 nS, which was 74·1 % of $g_{(GABA_A,peak)}$. *C*, superimposed traces of stimulation-evoked g_{GABA_A} (shown in Fig. 3*B*) and monosynaptic IPSP (shown in Fig. 2*B*). Both traces were normalized with respect to peak and polarity to enable temporal comparison. *D*, superimposition of scaled g_{GABA_A} and IPSC (shown in Fig. 2*C*).

g_{GABA_A} values were on average 2·1 nS (i.e. 13·8% of their peak value) in dendrites and 1·3 nS (i.e. 10·7% of peak) in somata (Table 1B).

Temporal comparison of orthodromic AP and g_{GABA_A}. In 3 of 14 dendritic and 4 of 11 somatic recordings, afferent stimulation elicited some suprathreshold responses at the selected stimulation intensities (Fig. 4*B*). Temporal comparison of latencies of APs and g_{GABA_A} in these cells showed near maximal expression of g_{GABA_A} at the time of onset of the synaptic APs: the average delay between AP onset and peak of g_{GABA_A} was 0·4 ± 0·2 ms ($n = 4$ somatic recordings). Values of $t_{(AP,onset)}$ and $t_{(peak,GABA_A)}$ correlated with $r = 0·82$. At $t_{(AP,onset)}$, g_{GABA_A} was on average 93·2 ± 9·4% of its peak (Table 1C). Similar values were obtained from dendritic recordings (Table 1B and C; Fig. 4*B*).

Components of monosynaptic inhibition

In a second approach, latency to onset of the evoked monosynaptic IPSP was obtained through the evaluation of its components: (a) antidromic AP in an interneuron (Fig. 5) and (b) unitary IPSP (Fig. 6). The values of latency to onset of the monosynaptic IPSP were similar in the two modes of measurements, i.e. via summation of components (Figs 5 and 6) and directly during pharmacological isolation (Figs 2–4, Table 1): the ranges of IPSP onsets were 1–3·9 ms (summation of components) and 1·7–3·9 ms (during isolation); the means were 2·6 ms (summation of components) and 2·8 ms (during isolation).

Antidromic action potentials in interneurons. In recordings of stratum pyramidale interneurons ($n = 7$) in the presence of CNQX (20–40 μM) and D-AP5 (50 μM), short-latency antidromic spikes could be elicited in two cases (Fig. 5*A–C*). Evidence for directly (as opposed to synaptically) evoked APs in these interneuron recordings is 3-fold. First, APs were elicited during blockade of excitatory transmission. Second, APs rose from the baseline in the absence of underlying EPSPs (Fig. 5*A*). Third, APs were elicited with short latencies (Fig. 5*A*): 0·4–0·7 ms (onsets) and 0·8–1·6 ms (peaks). In contrast, latencies to onset of synaptically evoked APs were > 2·5 ms in all interneuron recordings ($n = 28$) (Figs 8, 9 and 11).

As shown in Fig. 5*C*, the probability of eliciting antidromic interneuron APs is a function of (a) distance between stimulation and recording site, and (b) stimulation intensity. Antidromic APs could be elicited at relatively low stimulation intensities (50 μA in the cell shown in Fig. 5). With regard to distance, the percentage of antidromic spikes dropped to about 50% when the stimulation electrode was moved to a 1000 μm distance (compared with a 500 μm distance between stimulation and recording site; Fig. 5*C*). Latencies to onset of antidromic APs in the recording depicted in Fig. 5 increased from an average 0·42 ms (at 500 μm distance) to 0·78 ms (at 1000 μm). These values of $t_{(I,anti\text{-}AP,onset)}$ translate into velocities of AP propagation in interneuron axons of 1·39 mm ms^{-1}.

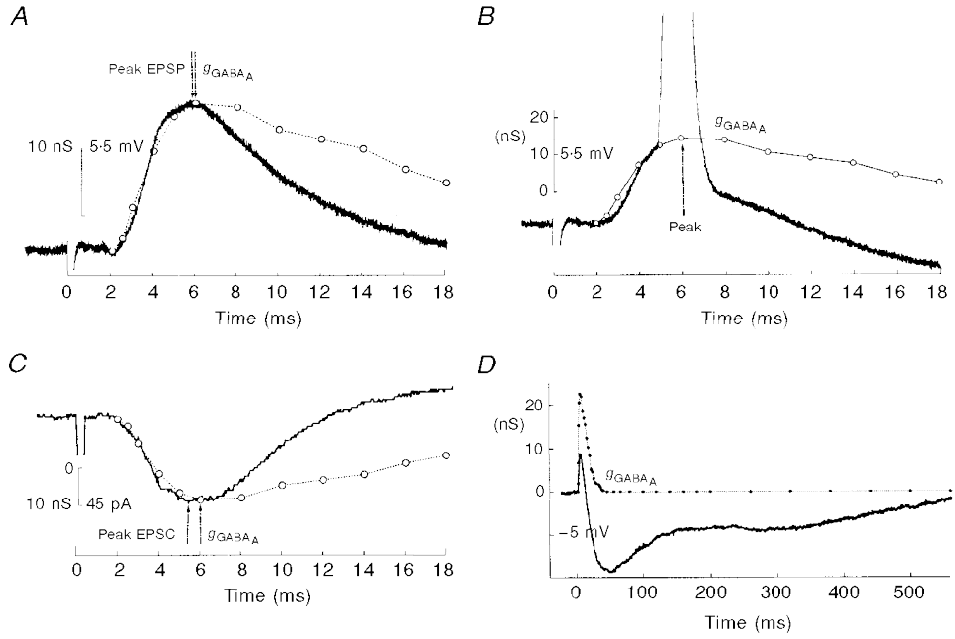

Figure 4. Temporal comparison of g_{GABA_A} and orthodromic EPSP/EPSC

A–C, superimposed traces (shown up to poststimulation $t = 18$ ms) of g_{GABA_A} and EPSP (*A*), g_{GABA_A} and suprathreshold EPSP (*B*), and g_{GABA_A} and EPSC (*C*). All traces were scaled to the same peak amplitude and polarity. *D*, superimposition of g_{GABA_A} and the entire orthodromic response. Amplitude scalings in *D* were arbitrarily chosen to allow clear separation of postsynaptic potential and g_{GABA_A}. All recordings and calculations were obtained from the same CA1 apical dendrite shown in Fig. 2 (EPSP/EPSC) and Fig. 3 (g_{GABA_A}).

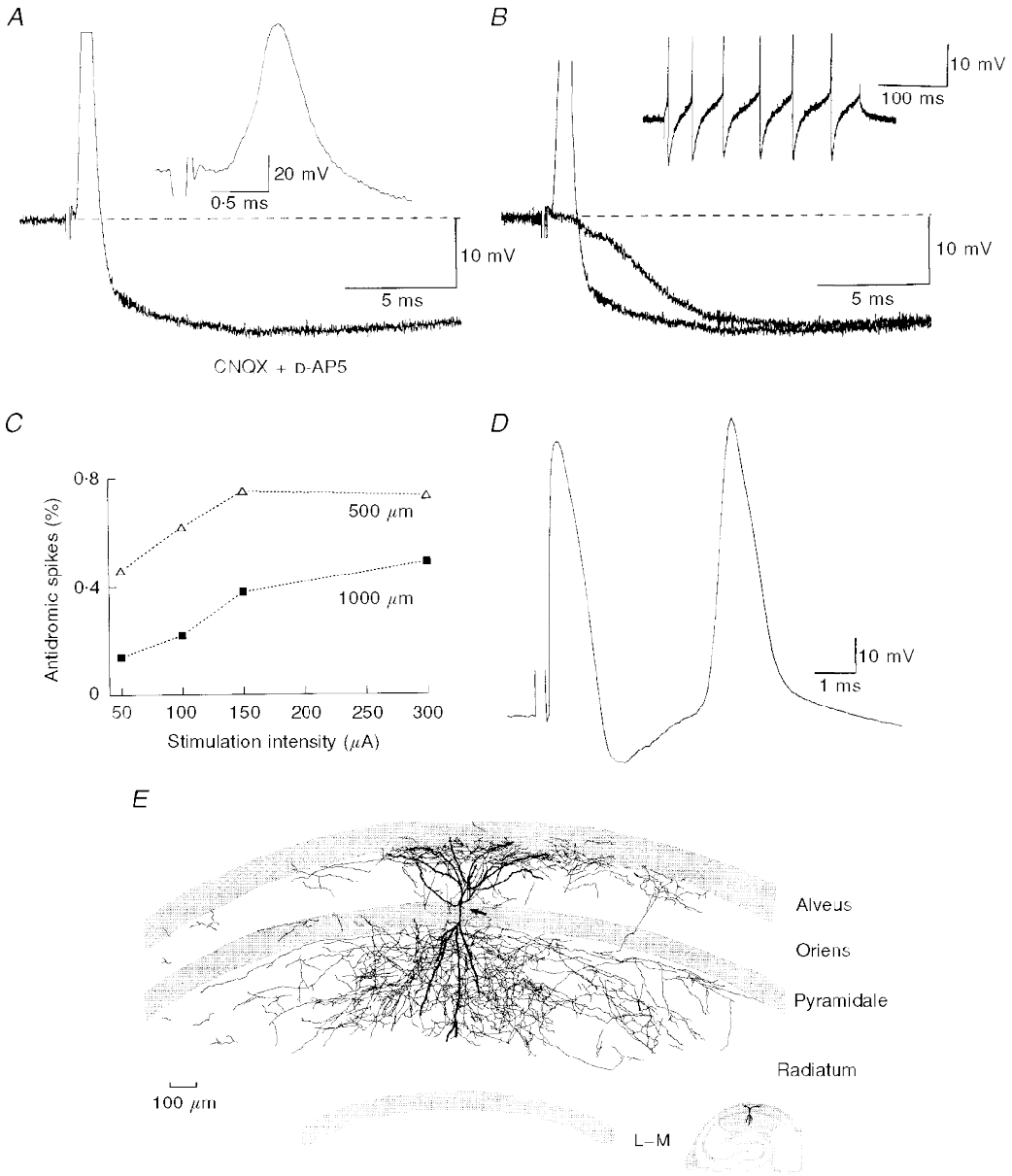

Figure 5. Antidromic APs and physiological properties in interneurons

A–C, intracellular recording of an interneuron (identified by physiological properties) in the presence of CNQX (40 μM) and D-AP5 (50 μM). *A*, stimulation elicited short-latency AP (truncated; shown in full in inset on enlarged time scale). *B*, superimposed recordings of antidromic AP and monosynaptic IPSP in the absence of antidromic AP. Both recordings were obtained consecutively under the same conditions (at V_{rest} −65 mV, 100 μA stimulation intensity). Latencies of the monosynaptic IPSP were: $t_{(I,IPSP,onset)}$, 1·68 ms; $t_{(I,IPSP,peak)}$, 11·96 ms. Superimposed recordings show that the hyperpolarization following the spike is composed of two components, a fast AHP that peaked at 1·89 ms (also seen in response to current injection, inset in *B*) followed by a larger, delayed monosynaptic IPSP. Inset: responses to current injection (300 ms, +0·2 nA at V_{rest} −65 mV). AP properties (averaged values): frequency of spike firing upon 0·2 nA current injection at V_{rest}, 22·4 Hz; $t_{(I,anti\text{-}AP,onset)}$, 0·47 ms (measured from the first leg of the stimulation artifact); $t_{(I,anti\text{-}AP,peak)}$, 0·925 ms; AP duration at half-width, 0·39 ms; at base, 1·04 ms; AHP, 9·8 mV (at V_{rest}). *C*, probability of (antidromic) spike elicitation as a function of stimulation intensity measured at two distances between stimulation and recording electrodes: 0·5 and 1 mm after repositioning of stimulation electrode. Averaged values are based on 15–23 recordings from the cell shown in *A* and *B*. Frequency of stimulation was 0·025 Hz. *D*, antidromic and orthodromic APs in a different interneuron (bistratified cell). Stimulation in stratum radiatum (distance to recording, 500 μm) produced two consecutive APs with poststimulation latencies to onsets of 0·4 and 5·3 ms, respectively. Duration at half-amplitude was 0·7 ms in antidromic and synaptic AP; AP height, 77 mV; AHP (of antidromic spike), −13·5 mV; recordings at V_{rest} −61 mV; R_{in}, 67 MΩ. *E*, camera lucida reconstruction of a bistratified cell recorded with a biocytin-

Table 2. Properties of dendritic unitary IPSPs

	Amplitude (mV)	Latency to onset (ms)	Rise time (10–90 %) (ms)	Duration at half-amplitude (ms)
Pair 1 ($n = 72$)	$1{\cdot}4 \pm 0{\cdot}3$	$0{\cdot}9 \pm 0{\cdot}1$	$2{\cdot}8 \pm 0{\cdot}3$	$24{\cdot}6 \pm 1{\cdot}6$
Pair 2 ($n = 11$)	$0{\cdot}9 \pm 0{\cdot}3$	$1{\cdot}7 \pm 0{\cdot}6$	$8{\cdot}0 \pm 1{\cdot}1$	$47{\cdot}8 \pm 8{\cdot}1$
Pair 3 (average of 22 traces)	0·4	2·3	12·7	55·5

IPSPs were recorded in CA1 pyramidal cell apical dendrites that were synaptically coupled to histologically identified bistratified cells. Data from 3 different pairs are listed separately (pairs 1–3). Analysis of pairs 1 and 2 is based on individual IPSPs (see Fig. 7); analysis of pair 3 is based on averaged traces (see Fig. 11*A*). Strong coupling was observed in pair 1 (no failure in response to single interneuron AP), and weak coupling in pair 3 (only averaged traces revealed IPSPs in response to a single interneuron AP). Synaptic coupling of pair 2 was of intermediate strength (single IPSPs in response to a single interneuron AP were detectable in 61 %). Criteria for coupling strength were IPSP amplitude and probability of elicitation in response to a single interneuron AP (or failure). The detection criterion for IPSPs was $> 0{\cdot}2$ mV hyperpolarization within 4 ms following the AP peak in the presynaptic interneuron. The 0·2 mV limit was based on the size of random membrane fluctations (noise), and the 4 ms latency limit was based on the maximal latency to onset of a clearly distinguishable IPSP.

In two bistratified cell recordings obtained under control conditions (i.e. in the presence of excitation), both antidromic and synaptic APs were clearly distinguishable (Fig. 5*D*). The delay between peaks ($\Delta t_{\text{(I,anti-AP,peak)– I,ortho-AP,peak)}}$) ranged from 2·3 to 10·4 ms (mean ± S.E.M., $4{\cdot}7 \pm 1{\cdot}6$ ms).

Unitary IPSPs in pyramidal cell dendrites. Out of 194 dual recordings of CA1 pyramidal cell apical dendrites and stratum pyramidale interneurons, unitary IPSPs were generated in three cases, all involving a bistratified cell (Figs 6, 11*Ac* and 13; Table 2).

The three pairs exhibited widely different strengths of coupling (Table 2). In one strongly connected pair of cells (shown in Fig. 6), prominent dendritic IPSPs (mean, $1{\cdot}4 \pm 0{\cdot}3$ mV, $n = 72$) were elicited without failure in response to single spikes in the presynaptic interneuron (Fig. 6*A* and *B*). In the weakly coupled pair (pair 3 in Table 2), IPSPs were only detectable upon averaging of several sweeps (Fig. 11*A c*) or in response to firing of interneuron AP doublets or triplets (see Fig. 13*B* and *C*). In pair 2, coupling strength was somewhere in between strong and weak: detectable ($> 0{\cdot}2$ mV) IPSPs (mean amplitude, $0{\cdot}9 \pm 0{\cdot}3$ mV) in response to single APs were revealed in 61 % of recordings (41/67).

As shown in Fig. 6 and Table 2, kinetics of dendritic unitary IPSPs recorded in the strongly coupled pair were as fast as perisomatic unitary IPSPs. Similar to unitary somatic IPSPs in strongly coupled cells, large variations in amplitude (Fig. 6*C*) and onset (Fig. 6*D*) and poor correlation between these two parameters were observed (Fig. 6*E*; see (Miles, 1990*b*). Unitary IPSP kinetics in weakly coupled dendritic recordings were considerably slower (Table 2): latencies to IPSP onset ($\Delta t_{\text{(I,AP,peak–P,IPSP,onset)}}$) in the weakly coupled cell were more than twice as long (> 2 ms) as those measured in the strongly coupled cell (Table 2). IPSP kinetics in pair 2 were in between those of strongly (pair 1) and weakly (pair 3) coupled cells. These data indicate a (negative) correlation between the strength of synaptic coupling and speed of IPSP kinetics.

Feedforward inhibition

Dual recordings of pyramidal cells and stratum pyramidale interneurons ($n = 17$) were carried out to determine the latencies to onset of feedforward IPSPs (Fig. 7). As shown in Fig. 7*A*, the onset of the feedforward IPSP was determined by the sum of components: (i) latency to peak of orthodromic APs in interneurons ($t_{\text{(I,ortho-AP,peak)}}$) (Fig. 7*A a*), and (ii) latency to onset of the unitary IPSP in the pyramidal

filled electrode in stratum pyramidale of the CA1 hippocampal subfield. The reconstruction is based on 6 successive 60 μm sections of the hippocampal slice. The inset shows the abbreviated dendritic arbor and the location of the cell within CA1. The shaded area in the inset represents the segment shown in full. The arrow depicts the initial axonal segment arising from the soma–apical dendrite junction. Dendritic arborization is depicted by the thick lines, and axonal arborization by the thin lines. Axonal arbor in strata radiatum and oriens extended about 1200 μm in either transversal direction of the slice. Some details (e.g. dendritic beading and axonal synaptic boutons) were omitted in the reconstruction. L–M, lacunosum–moleculare.

Table 3. Properties of CA1 neurons

A.	Pyramidal cells	Interneurons	Statistics
V_{rest} (mV)	−64·5 ± 1·3 (n = 17)	−66·2 ± 2·2 (n = 17)	
AP threshold (mV)	−53·2 ± 2·1 (n = 17)	−55·4 ± 1·9 (n = 17)	
$t_{(EPSP,onset)}$	2·9 ± 0·3 (n = 17)	2·7 ± 0·5 (n = 17)	
EPSP slope (mV ms^{-1})	1·6 ± 0·4 (n = 17)	4·0 ± 0·7 (n = 17)	*
τ_m (ms)	21·1 ± 1·2 (n = 17)	16·2 ± 1·5 (n = 17)	*
R_{in}	53·3 ± 7·7 (n = 17)	96·9 ± 10·7 (n = 17)	*

B.	I cells (n = 28)	Basket cells (n = 15)	Axo-axonic cells (n = 6)	Bistratified cells (n = 7)
$t_{(EPSP,onset)}$	2·7 ± 0·3	2·8 ± 0·5	2·4 ± 0·6	2·7 ± 0·4
$t_{(EPSP,peak)}$	5·6 ± 0·5	5·8 ± 0·7	5·0 ± 1·1	5·9 ± 0·6
$t_{(AP,onset)}$	5·3 ± 0·3	5·7 ± 0·9	4·8 ± 1·2	5·2 ± 0·5
$t_{(AP,peak)}$	5·8 ± 0·3	6·1 ± 0·7	5·2 ± 1·0	5·8 ± 0·7

A, properties of pyramidal cells and stratum pyramidale interneurons recorded simultaneously. B, activation kinetics in CA1 stratum pyramidale interneurons (total, n = 28; and various subtypes). * indicates significant difference between pyramidal cell and interneuron values ($P < 0·05$, Student's t test).

cell ($\Delta t_{(I,AP,peak\text{-}P,IPSP,onset)}$) (Fig. 7*Ab*). A 1 ms constant was generally substituted for $\Delta t_{(I,AP,peak-P,IPSP,onset)}$ in non-coupled pairs (see Fig. 7*A*).

The temporal overlap between feedforward inhibition and orthodromic EPSP in pyramidal cells was measured by projecting the latency of the feedforward IPSP onto the orthodromic EPSP elicited in the simultaneously recorded pyramidal cell (Fig. 7*B*). Onsets of the feedforward IPSP occurred in 13 of 17 dual recordings during the EPSP rising phase. Temporal overlap was quantified by a scale defined by onset (assigned value '1') and peak of the pyramidal cell EPSP (assigned value '0') (see legend to Fig. 7). By this

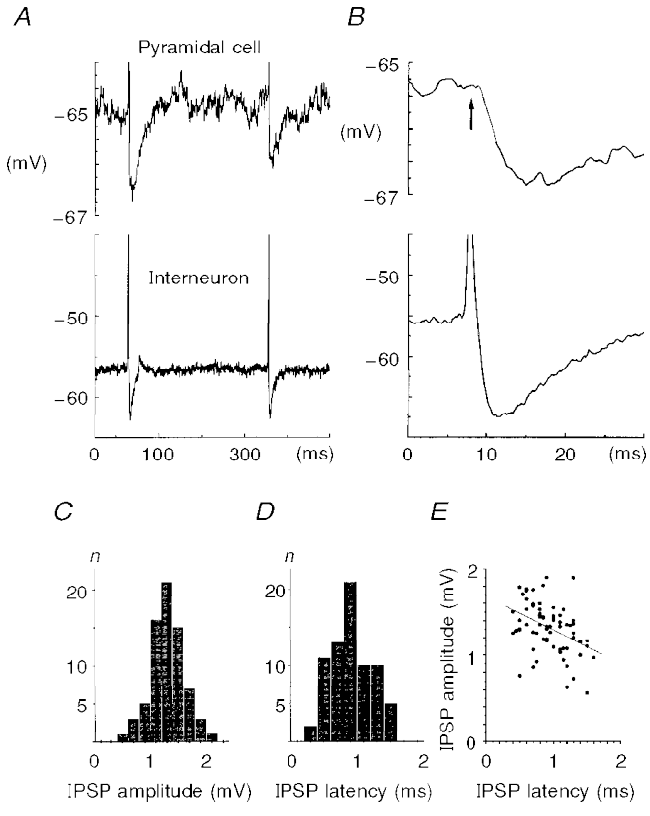

Figure 6. Characteristics of unitary IPSPs recorded in a CA1 pyramidal cell dendrite

Paired recording of a bistratified cell (recorded in stratum pyramidale) and pyramidal cell apical dendrite (recorded in stratum radiatum, 250 μm from stratum pyramidale). *A*, single spontaneous spikes in the interneuron (lower trace) elicited corresponding IPSPs in the simultaneously recorded pyramidal cell (upper trace; filtered at 0·3 kHz) without failure. All recordings were carried out at respective V_{rest} (−65 mV in pyramidal cell dendrite, −58 mV in interneuron). *B*, single interneuron AP and corresponding IPSP on an extended time scale. Peak amplitude of the IPSP in the depicted recording was 1·48 mV, latency to onset (from AP peak of interneuron) was 0·97 ms, rise time (10–90 %) was 3·6 ms, and duration at half-amplitude was 21 ms. *C*, distribution of IPSP amplitudes ranging from 0·4 to 2·2 mV (bin width, 0·2 mV). *D*, distribution of latency to onset (measured from peak of AP in presynaptic interneuron) ranging from 0·2 to 1·6 ms (bin width, 0·2 ms; n = 72). *E*, linear regression analysis of IPSP amplitude and latency (same values as shown in *C* and *D*) shows poor correlation between the two parameters ($r = -0·39$; n = 72, $P > 0·066$). Cell characteristics (means): interneuron: spike width at half-amplitude, 0·55 ms; AHP (peak), −18 mV; R_{in}, 83 MΩ; dendrite: spike width at half-amplitude, 1·25 ms; R_{in}, 39 MΩ.

measure, temporal overlap ranged from 0·75 (i.e. feedforward inhibition was present during 75% of the EPSP rising phase) to −0·21 (i.e. feedforward inhibition started during the early decay phase of the EPSP). On average (all interneurons taken together, $n = 17$), the onset of the feedforward inhibitory response coincided with the last quarter of the EPSP rising phase (factor 0·255). Slightly faster onsets of feedforward inhibition were mediated by axo-axonic cells (mean overlap, $0{\cdot}43 \pm 0{\cdot}22$) compared with those of bistratified cells (mean overlap, $0{\cdot}20 \pm 0{\cdot}1$) and basket cells (mean overlap, $0{\cdot}23 \pm 0{\cdot}1$).

In Fig. 7*C*, the values of feedfoward IPSP onset (measured in the interneurons of the 17 pairs shown in Fig. 7*B*), were projected onto a standard EPSP (2·8 ms latency to onset and 7·8 ms latency to peak: these values were the average from 39 dendritic and 24 somatic pyramidal cell recordings). Comparing Fig. 7*B* and *C* shows that the distribution of feedforward IPSP onsets was similar. Using the standard EPSP (as in Fig. 7*C*), a measure of feedforward inhibition can be obtained from single interneuron recordings (e.g. from the basket cell shown in Fig. 9 and recordings of Lucifer Yellow-stained interneurons from a previous study (Stelzer *et al.* 1994). The calculated values of temporal overlap feedforward IPSP–orthodromic EPSP based on all interneuron recordings ($n = 37$; shown in Fig. 7*D*) confirm the results of the smaller stratum pyramidale interneuron population ($n = 17$; shown in Fig. 7*C*): in 31 of 37 comparisons of stratum pyramidale interneuron-mediated IPSPs, feedforward inhibition occurred during the rising phase of the average pyramidal cell EPSP.

A very similar distribution was seen for IPSPs mediated by stratum lacunosum–moleculare (L–M) interneurons: in 10 of 14 recordings, L–M-mediated IPSPs coincided with the EPSP rising phase, and 4 of 14 with the early decay phase of the averaged EPSP.

IPSP onsets obtained from alveus–oriens (A–O) interneuron recordings were significantly slower (Fig. 7*D*). In 6 of 7 A–O

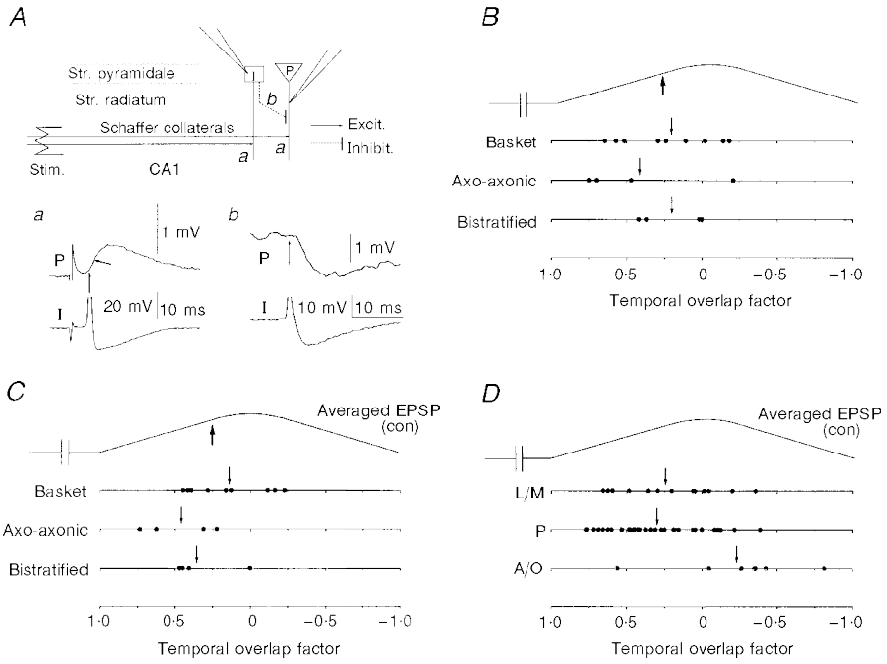

Figure 7. Onsets of feedforward IPSP in CA1 pyramidal cell dendrites

A, experimental protocol of assessing onset of feedforward IPSPs in pyramidal cells. Onset of feedforward inhibition was determined by summation of its underlying components: in concomitant recordings of pyramidal cell dendrite and stratum pyramidale interneuron, latency to peak of synaptic interneuron AP (I) ($t_{(\mathrm{I,ortho\text{-}AP,peak})}$) (*a*) and onset of unitary IPSP ($\Delta t_{(\mathrm{I,AP,peak-P,IPSP,onset})}$) (*b*) were measured. The sum of the latency of both components was projected onto the EPSP of the concomitantly recorded pyramidal cell (oblique arrow in *a*). In non-coupled pairs, a 1 ms value was used for $\Delta t_{(\mathrm{I,AP,peak-P,IPSP,onset})}$. *B*, dots denote the calculated values of feedforward IPSP in temporal relation to the EPSP of the concomitantly recorded pyramidal cell ($n = 17$ pairs). In *C*, the same values of latencies to onset of the feedforward IPSP (measured in the interneurons of the 17 pairs shown in *B*), were projected onto an EPSP whose latencies to onset and peak represent the mean values of several pyramidal cell recordings. *D*, calculated onsets of feedforward inhibition from all interneuron recordings are shown in temporal comparison with the averaged EPSP. In *B* and *C*, a small arrow denotes the mean value in each group, the larger arrow (pointing towards the EPSP) represents the mean value of all 17 recordings. The number scale (at the bottom of *B*–*D*) was defined by the pyramidal cell EPSP onset and peak: the value '1·0' was assigned to onset, the value '0' to peak, and negative values accordingly to EPSP decay.

interneurons, IPSP onsets coincided with the decay phase of the EPSP, and in only 1 of 7 with the EPSP rising phase. Furthermore, the mean of temporal overlap between A–O cell-mediated IPSPs and the EPSP ($-0{\cdot}24 \pm 0{\cdot}16$) was significantly different from that of pyramidale interneurons ($0{\cdot}30 \pm 0{\cdot}05$; $P < 0{\cdot}002$, ANOVA) and L–M interneurons ($0{\cdot}24 \pm 0{\cdot}09$; $P < 0{\cdot}01$). The late onset of A–O cell-mediated IPSPs is probably due to the fact that A–O interneuron activation was implemented via recurrent excitation through CA1 pyramidal cell APs (Blasco-Ibanez & Freund, 1995; Maccaferri & McBain, 1995). This notion is supported by the delayed onset of the stimulation-evoked EPSP in A–O interneurons ($6{\cdot}4 \pm 1{\cdot}3$ ms, mean ± S.E.M., $n = 7$). In comparison, mean onset of orthodromic EPSPs in stratum pyramidale interneurons was $2{\cdot}7 \pm 0{\cdot}3$ ms ($n = 28$; Table 3B).

Differential excitability of interneurons and pyramidal cells

The protocol of comparing time courses of feedforward inhibition and EPSP required the concomitant elicitation of synaptic APs in the interneuron, but subthreshold EPSPs in the pyramidal cell (Fig. 7*A*). This condition was met in a large range of stimulation intensities due to differential excitability of interneurons and pyramidal cells (Scharfman,

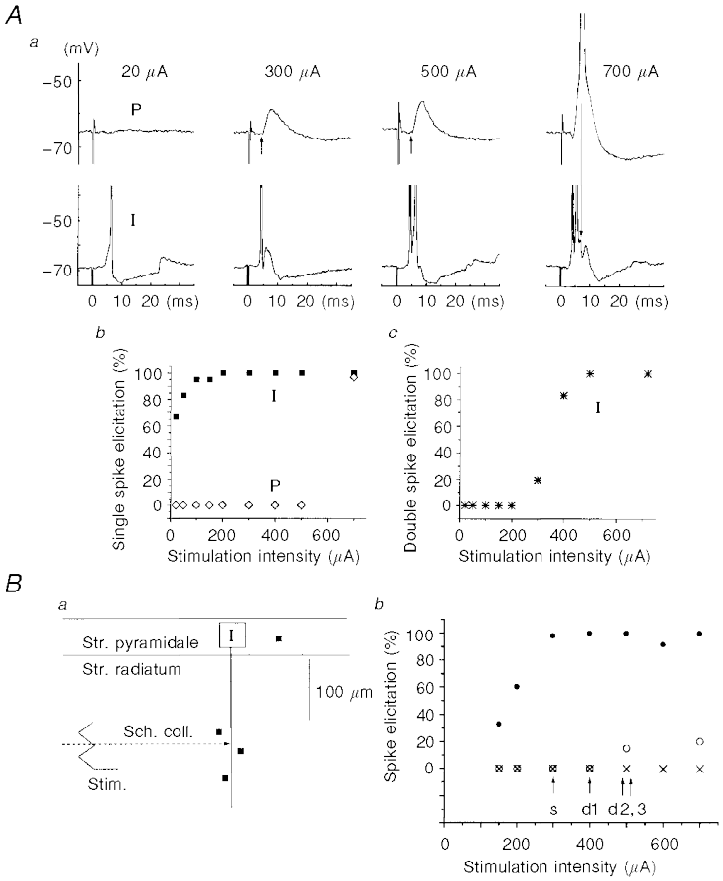

Figure 8. Elicitation of synaptic APs in interneurons and pyramidal cells

Aa, concomitant recordings at four representative stimulation intensities (20, 300, 500 and 700 μA) in an axo-axonic cell and pyramidal cell apical dendrite. *Ab*, plot of spike elicitation probability *versus* stimulation intensity. *Ac*, plot of probability of double spike elicitation in interneurons as a function of stimulation intensity. Analysis is based on 6–12 recordings at each stimulation intensity. Arrows at 300 and 500 μA (in *a*) depict the sum of latencies of interneuron spike plus 0·2 ms. Cellular properties: R_{in}, bistratified cell, 38 MΩ; pyramidal cell, 21 MΩ; V_{rest}, bistratified cell, −63 mV; pyramidal cell, −65 mV; spike width at half-amplitude in bistratified cell, 0·45 ms; AHP, −16 mV. *B*, comparison of spike elicitation probability in basket cell and four pyramidal cells (three apical dendrites, one soma) that were consecutively recorded in combination with the basket cell. Orthodromic responses were elicited at various stimulation intensities (from 150 to 700 μA) for each of the four basket cell–pyramidal cell pairs. *Ba*, schematic depiction of interneuron and pyramidal cell recording sites. *Bb*, probabilities of spike elicitation in basket cell (●), soma (○) and dendrites (×). Arrows mark the stimulation intensity at which pyramidal cells exhibited half-maximal EPSP peak amplitudes. Cellular properties: R_{in}, basket cell, 96 MΩ; pyramidal cells, 41 ± 9 MΩ (mean ± S.E.M., $n = 3$); V_{rest}, basket cell, −72 mV; pyramidal cells, -64 ± 3 mV; spike width at half-amplitude in interneuron, 0·5 ms; AHP, −14 mV.

1991). For example, in the paired recording shown in Fig. 8*A*, synaptic spikes in the axo-axonic cell were elicited at 20 μA, whereas > 500 μA was required for synaptic spikes in the concomitantly recorded pyramidal cell dendrite. In addition, double spike responses in the interneuron were accompanied by subthreshold EPSP responses in the pyramidal cell over a large range of stimulation intensities (Fig. 8*Ac*). In Fig. 8*B*, probabilities of synaptic spikes were compared in a basket cell and four pyramidal cells (3 dendrites and 1 soma) that were recorded consecutively during the same interneuron recording. The basket cell responded with synaptic APs at any intensity (with 100% probability at intensities > 300 μA). In contrast, none of the three concomitantly recorded pyramidal cell dendrites exhibited spike responses at any of the selected stimulation intensities. In the pyramidal cell soma, 10–20% of synaptic APs were observed at intensities of 500 and 700 μA, respectively.

It seems that in CA1 pyramidal cells – similar to neocortical pyramidal cells (Ling & Benardo, 1998) – the magnitude of inhibitory responses reaches an upper limit at stimulation intensities at which excitation is far below its maximum. In the dual recordings shown in Fig. 8*A* and *B*, interneurons responded in all recordings with synaptic spikes at the stimulation intensities that elicited half-maximal EPSPs in the pyramidal cells (at 300 μA in Fig. 8*A*; marked by arrows in Fig. 8*Bb*). With stimulation intensities adjusted to generate about half-maximal EPSPs in the pyramidal cells (e.g. in the experiments shown in Fig. 7), synaptic interneuron APs were elicited in 57 of 62 pairs (in 39 of 57 cases with a 100% probability, in 18 cases with probabilities between 34 and 90%). Taken together, these data show that maximal efficacy of feedforward inhibition is reached by stimulation intensities that generate only about 50% of maximal EPSPs in pyramidal cells.

Temporal overlap of feedforward inhibition and EPSP: role of stimulation intensity

As shown in Fig. 8*A* (at 20 μA), synaptic interneuron APs could be elicited at stimulation intensities that were below the threshold for eliciting pyramidal cell EPSPs. This was observed in 16 of 24 combinations of interneuron–pyramidal cell recordings at which such low intensities were applied. These data demonstrate that the weakest excitatory input into CA1 is accompanied by large activation of the feedforward inhibitory pathway. What is the temporal overlap between feedforward inhibition and evoked excitation for such weak excitatory input?

Activation kinetics changed with increasing stimulation intensity in both interneurons (Lacaille, 1991) (Fig. 9*E*) and pyramidal cells (Fig. 10*E*). As illustrated in Fig. 9 in a single interneuron recording, the decrease in $t_{(I,AP,peak)}$ (Fig. 9*D*) was accompanied by a parallel increase in the slope of the orthodromic EPSP (Fig. 9*C* and *F*). However, the changes of interneuron kinetics do not generally result in a change of temporal overlap between feedforward inhibition and evoked excitation in the pyramidal cell. This is illustrated in Fig. 10. There was a close correlation between latencies to peaks of interneuron APs ($t_{(I,AP,peak)}$; Fig. 10*B*) and latencies to EPSP peak in pyramidal cells (Fig. 10*A*). As a result, the difference of $t_{(P,EPSP,peak)}$ and $t_{(I,AP,peak)}$ (Fig. 10*C*) and temporal overlap of feedforward inhibition and orthodromic excitation (Fig. 10*F*) were

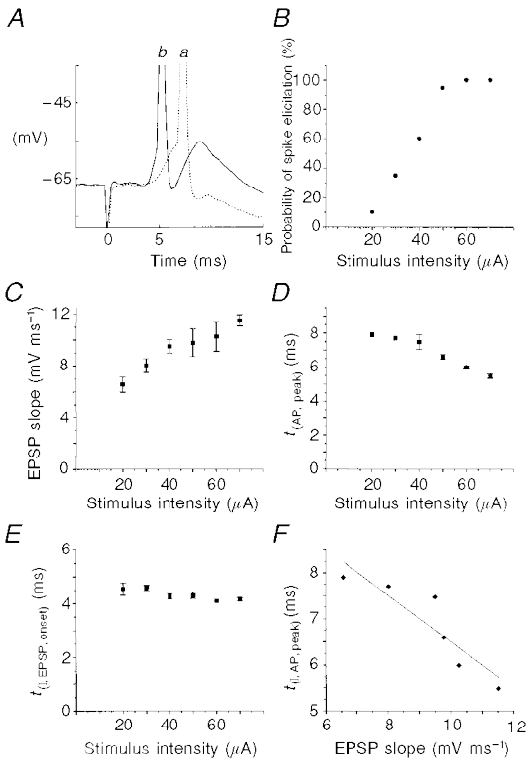

Figure 9. Kinetics of interneuron excitation change with increasing stimulation intensity

Orthodromically evoked excitatory responses in single CA1 basket cell recordings at V_{rest} (−66 mV). Distance between stimulation and perpendicular line through stratum pyramidale recording site was ~700 μm, spike threshold was −56 mV. *A*, representative recordings of orthodromic responses in basket cell at 30 μA (*a*) and 70 μA (*b*) stimulation intensities. EPSP slope: 5·3 mV ms^{-1} at 30 μA (*a*), 10·6 mV ms^{-1} at 70 μA (*b*); $t_{(I,AP,peak)}$, 7·3 ms (*a*) and 5·4 ms (*b*); $t_{(EPSP,onset)}$, 4·4 ms (*a*), 4·1 ms (*b*). *B*, probability of orthodromic spike elicitation as a function of stimulation intensity. *C*, EPSP slope as function of stimulation intensity. *D*, plot of $t_{(I,AP,peak)}$ as function of stimulation intensity. *E*, $t_{(I,EPSP,onset)}$ as function of stimulation intensity. *F*, linear regression of EPSP slope and $t_{(I,AP,peak)}$. Mean values of $t_{(I,AP\ peak)}$ and EPSP slope were different (Student's *t* test, comparison of means measured at 20 and 70 μA, respectively); EPSP onset was not. Analysis in *B*, *C* and *E* is based on 20 recordings at each stimulation intensity; analysis in *D* and *F* is based on the suprathreshold recordings in the same basket cell.

similar in the entire range of stimulation. Latencies to onset were not generally affected by stimulation intensity (Figs 9*E* and 10*E*). These data show that the high degree of temporal overlap between feedforward inhibition and excitation – measured at half-maximal EPSPs (Fig. 7) – is also seen at lower stimulation intensities and smaller EPSPs.

Recurrent inhibition

The time course of the recurrent inhibitory response was evaluated via measurements of its underlying components (Fig. 11): (1) latency to peak of synaptic pyramidal cell AP ($t_{(P,AP,peak)}$; Fig. 11*Aa*, P); (2) latency between pyramidal cell AP peak and unitary AP peak in a coupled interneuron ($\Delta t_{(P,AP,peak–I,unitaryAP,peak)}$; Figs 11*Ab* and 12*A* and *B*); (3) latency between interneuron AP peak and onset of unitary IPSP in the pyramidal cell ($\Delta t_{(I,AP,peak–P,mono-IPSP,onset)}$; Fig. 11*Ac*).

The results of this approach can be summarized as follows (see below for details). First, the earliest onsets of the recurrent IPSP occur several milliseconds (> 3 ms) after the peak of the orthodromic EPSP in pyramidal cells. Thus recurrent inhibition is not a factor in the control of the EPSP rising phase. Second, recurrent inhibitory responses are prominently expressed at the time of the peak of the orthodromic population IPSP: in the recordings of Figs 11–13, earliest onsets of recurrent inhibition occurred at poststimulation latency $t = 11$ ms (see Fig. 11*B*); the peak of the population IPSP was measured at $t = 26$ ms. Third, a widespread range of recurrent IPSP onsets (in the pyramidal cell shown in Figs 11–13 from 11 to 99·8 ms; see Fig. 11*B*) were observed.

Measurements of all three components could be obtained from a mutually coupled bistratified cell and pyramidal cell apical dendrite (Figs 11–13). In this pair, strong coupling was observed between the pyramidal cell and the interneuron: pyramidal cell APs elicited large unitary EPSP without failure (in many cases suprathreshold) in the interneuron (Fig. 12). In reverse, the interneuron was (albeit weakly) coupled to the recorded dendrite (Fig. 13). The onsets of mono- and feedforward IPSPs in relation to the pyramidal cell EPSP in this pair (Fig. 11*B*) were in the general range of respective onsets seen in other cells (see Figs 2 and 7).

Latencies to peak of pyramidal cell AP

In pyramidal cells, the latencies to peaks of synaptic APs (component *a*, Fig. 11*A*) coincided roughly with the latencies to their EPSP peaks (e.g. Fig. 4*B*; Table 1B for single recordings; Figs 8*A* and 11*A* for dual recordings). In the pyramidal cell of the dual recording shown in Figs 11–13, mean latency to synaptic AP peak was 9·8 ± 0·3 ms ($n = 27$; range 8·6–11·4 ms; Figs 11*Aa* and 12*D*); mean latency to EPSP peak was 9·4 ± 1·1 ms ($n = 12$, range 5·6–12·0 ms). Since the onset of recurrent inhibition starts several milliseconds after the EPSP peak (i.e. the delay is the sum of components *b* and *c*, see below), it is clear that recurrent inhibitory influences are not present during the slope or peak of the orthodromic EPSP.

Latencies of recurrent disynaptic IPSPs

Component *b*. Strong coupling between the pyramidal cell and the interneuron (Figs 11 and 12) allowed measurements of (a) latencies to onset of unitary EPSPs that ranged from 0·4 to 1·5 ms (mean, 1·04 ± 0·07 ms, $n = 268$); and

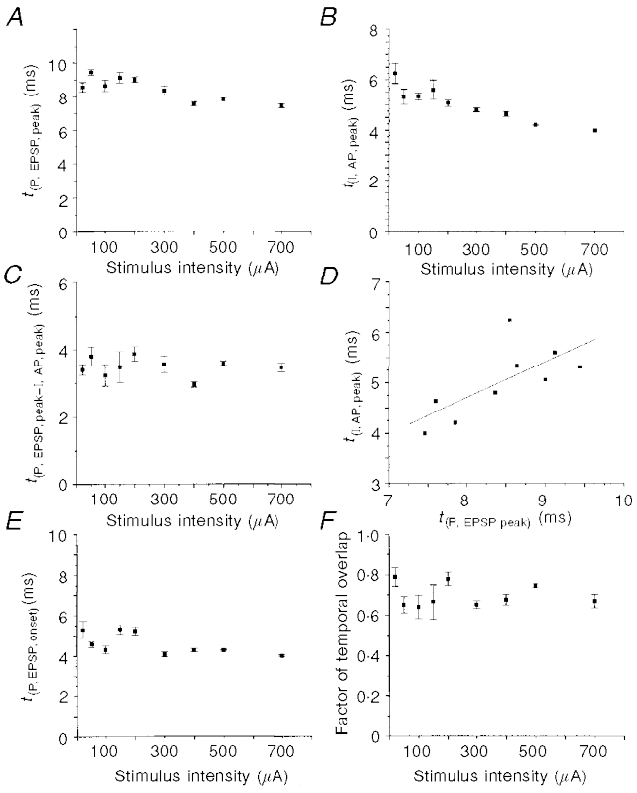

Figure 10. Degree of temporal overlap between feedforward inhibition and pyramidal cell EPSP as a function of stimulation intensity

A, kinetic parameters that determine temporal overlap between feedforward inhibition and pyramidal cell EPSP. $t_{(P,EPSP,peak)}$ (*A*) and $t_{(I,AP,peak)}$ (*B*) exhibited similar decreases in the selected stimulation range. Correlation coefficient between $t_{(P,EPSP,peak)}$ and $t_{(I,AP,peak)}$ (*C*) was $r = 0·7$. *D*, the difference between pyramidal cell EPSP peak and AP peak in interneuron remained unchanged by increased stimulation. *E*, $t_{(P,EPSP,onset)}$ was variable, but not changed. *F*, temporal overlap between onset of feedforward inhibition and EPSP was statistically the same in the depicted stimulation range. Data were calculated from the dual recording of pyramidal cell dendrite and axo-axonic cell shown in Fig. 8*A*.

(b) latencies to unitary AP peaks in the interneuron ($\Delta t_{(P,AP,peak-I,unitary\ AP,peak)}$). This parameter exhibited large variability, ranging from 2·6 to 86·4 ms (shown in histogram of Fig. 12*C*). Two types of unitary interneuron APs were observed (Fig. 12*B* and *C*): (a) early APs that rose during the EPSP rising phase (Fig. 12*Ba*); and (b) late APs that originated during the plateau phase of unitary EPSPs (Fig. 12*Bb*). Early APs ranged from 2·6 to 8·8 ms (mean ± S.E.M., 6·0 ± 0·2 ms, $n = 61$); latencies to late APs ranged from 6 to 86 ms (mean ± S.E.M., 30·8 ± 1·4 ms; $n = 174$).

Component *c*. Weak inhibitory coupling with the pyramidal cell was observed in the same pair of cells (Figs 11*Ac* and 13). A monosynaptic IPSP was revealed by averaging several traces (e.g. Fig. 11*Ac*) or in response to double and triple spikes in the presynaptic interneuron (Fig. 13). Latencies to onsets of IPSPs (apparently triggered by the second of multiple spikes, see Fig. 13) were on average 2·4 ± 0·4 ms ($n = 22$; range between 1·5 and 3·1 ms). In comparison, latency between interneuron AP peak and onset of the averaged ($n = 22$) monosynaptic IPSP in response to a single interneuron spike was 2·3 ms

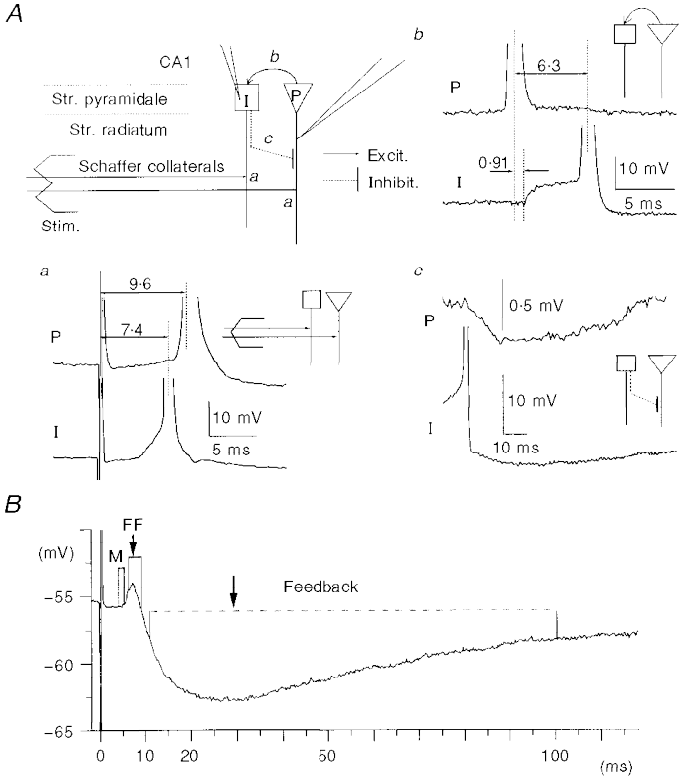

Figure 11. Onsets of recurrent IPSPs in a CA1 pyramidal cell dendrite

A, experimental protocol of measuring latencies to onset of recurrent IPSPs in a CA1 pyramidal cell. A schematic depiction of the feedback inhibitory pathway and recording arrangements in the CA1 hippocampal subfield is shown top left. The onset of the feedback inhibitory response was evaluated by separately measuring the three underlying components (*a*–*c*) in a mutually coupled pair of pyramidal cell (dendritic recording, 100 μm from stratum pyramidale) and interneuron (bistratified cell, recorded in stratum pyramidale). *a*, poststimulation latencies to peaks of synaptic APs in pyramidal cell (9·6 ms) and interneuron (7·4 ms in the recording depicted). *b*, measurements of latency between the pyramidal cell AP (spontaneously generated) and the interneuron AP on top of a unitary EPSP in the synaptically coupled interneuron (6·3 ms in the recording depicted, see Fig. 12). *c*, latency between interneuron AP peak and onset of the averaged ($n = 22$) monosynaptic IPSP in the coupled pyramidal cell was 2·3 ms. All recordings were obtained at respective V_{rest} (between −55 and −58 mV in pyramidal cell, −65 mV in interneuron). Duration of interneuron AP at half-width was 0·7 ms, AHP was 9 mV. The distance between the two cells in the transverse direction was 50 μm. Distances between stimulation and recording electrodes were about 1 mm. *B*, latencies to onset of the recurrent IPSP were calculated by summation of components *a*–*c*. The onset of the recurrent IPSP based on the summation of the three components was on average 29·4 ± 1·3 ms ($n = 235$; early and late APs taken together, see Fig. 13). Based on early APs alone, latencies to onset of feedback IPSPs were on average 16·0 ± 0·2 ms ($n = 61$); based on late APs alone, 38·9 ± 1·4 ms ($n = 174$). FF, range of onsets of feedforward IPSPs; M, onsets of monosynaptic IPSPs in the same pyramidal cell.

(Fig. 11*Ac*). The shortest latency of recurrent disynaptic IPSPs (sum of minima of components *b* and *c*) was 4·4 ms; the mean value was 8·3 ms (based on the short-latency unitary APs, Fig. 12*Ba* and *C*).

Summation of all three components of recurrent inhibition

The shortest latency to onset of the recurrent (trisynaptic) IPSP (sum of respective minima of components *a*–*c*) was 11·0 ms. The longest latency to onset (sum of respective maxima of components *a*–*c*) was 99·8 ms (Fig. 11*B*).

DISCUSSION

The main conclusions of this study are as follows.

(1) $GABA_A$-mediated inhibitory influences were present during the entire duration of the orthodromic EPSP/EPSC in CA1 pyramidal cells. Results show that the slope of the orthodromic EPSP is not a pure measure of excitation (cf. Wigström & Gustafsson, 1983), but controlled by fast synaptic inhibition (Figs 4, 7 and 8*A*). During the EPSP rising phase, the inhibitory influences came from the antidromic monosynaptic (Fig. 4) and feedforward (Figs 7

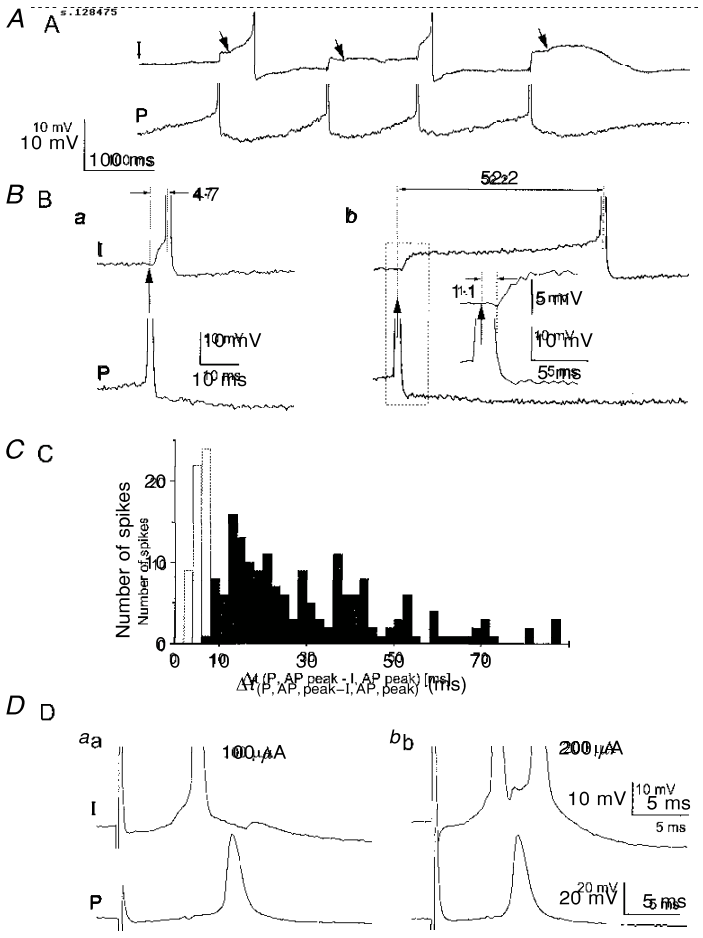

Figure 12. Properties of recurrent interneuron excitation

Properties of unitary EPSPs elicited in a bistratified cell (see Fig. 11). *A*, distinct EPSPs in the interneuron (I) were elicited by spontaneous APs in the concomitantly recorded pyramidal cell (P). The baseline membrane potential of the interneuron was tonically depolarized (from a V_{rest} value of −65 mV to −61 mV). Interneuron AHPs prevented some EPSPs to become suprathreshold, effectively filtering the roughly 15 Hz AP frequency in the pyramical cell to a 7·5 Hz rhythm of synaptic APs in the interneuron. Distinct superimposed EPSPs were observed in the interneuron (marked by arrows). *B*, typical examples of early (*a*, open bars in *C*) and late APs (*b*, filled bars in *C*) on top of unitary EPSPs. Numbers denote latencies between peaks of pyramidal cell AP and unitary EPSP-triggered APs in the coupled interneuron ($\Delta t_{(P,AP,\ peak-I,AP,peak)}$), 4·7 ms (*a*) and 52·6 ms (*b*). Latency to onset of unitary EPSP (inset on right) was 1·1 ms. *C*, distribution of $\Delta t_{(P,AP,peak-I,AP,peak)}$ ($n = 235$ measurements). The open bars depict latencies to early APs, filled bars latencies to delayed APs. *D*, orthodromic responses in the same pair of pyramidal cell and interneuron shown in *A*–*C*. Orthodromic responses in interneuron (top) and pyramidal cell (bottom) were obtained at 100 μA (*a*) and 200 μA (*b*). In *a*, the delayed pyramidal cell AP triggered a unitary EPSP with the typical delay (1·1 ms). In *b*, orthodromic stimulation elicited a double spike response in the interneuron. The peak of pyramidal cell AP preceded peak of the second interneuron spike by 2·5 ms.

and 8*A*) component. In contrast, onset of recurrent inhibition started several milliseconds after the EPSP peak (Fig. 11).

(2) Kinetics of $GABA_A$-mediated conductance changes were considerably faster than those of the IPSP or IPSC of the same evoked event (Table 1, Fig. 4). These data underline the pivotal role of the actions of inhibitory shunting in the control of excitatory input in CA1.

(3) Synaptic interneuron spikes could be elicited by stimulation intensities that were below the threshold of EPSP elicitation in the pyramidal cell (Fig. 8*A*). In addition, firing of a single pyramidal cell induced unitary interneuron APs (Fig. 12). These data indicate that weakest excitatory input into CA1, e.g. unitary pyramidal cell EPSPs (Turner, 1988; Sayer *et al.* 1989), activates CA1 interneurons in a feedforward manner. Feedforward inhibition exerted a high degree of temporal overlap with evoked excitation at any strength of excitatory input (Figs 7, 8 and 10). Taken together, these results suggest that *in situ*, any excitatory input in CA1 is controlled by fast synaptic inhibition.

Monosynaptic inhibition

Since the monosynaptic inhibitory response is elicited by direct electrical stimulation of interneuron processes (Fig. 5) and is therefore not observed *in situ*, the question arises as to why such detailed examination of the kinetics was carried out (Figs 2–5; Table 1). First, the orthodromic response of CA1 pyramidal cells is a frequently used experimental measure of excitability. The presented data (Figs 2–4; Table 1) show that – with monosynaptic inhibition being an integral component – $GABA_A$-mediated influences are present before the onset of the orthodromic EPSP in dendrites. Second, the monosynaptic inhibitory response could be isolated pharmacologically (Davies *et al.* 1990). It is inferred that the main finding regarding the kinetics of monosynaptic inhibition (g_{GABA_A} faster than IPSCs and IPSPs) applies also to feedforward and feedback inhibitory responses. Third, the similarity of latencies to IPSPs measured directly (Figs 2–4; Table 1) and indirectly via summation of components (Figs 5 and 6) demonstrated the feasibility of the indirect approach via summation of components. The latter was the sole approach in the evaluation of feedforward (Fig. 7) and feedback inhibition (Fig. 11).

Feedforward inhibition

The kinetics of interneuron activation reported here are in agreement with those reported previously: overall latency to disynaptic IPSPs (Miles, 1990*b*), poststimulation intervals to interneuron AP peaks (Lacaille, 1991; Scharfman, 1991), and differences in latency between interneuron and pyramidal cell firing (Ashwood *et al.* 1984). Kinetics of dendritic unitary IPSPs, however, were found to be faster in cases of strongly coupled cells (see Table 2) than reported previously (Miles, 1990*b*; Buhl *et al.* 1994*a*).

Data in Fig. 7*B–D* show that fastest feedforward inhibitory responses cover 75% of the EPSP rising phase. There is convincing evidence that onsets of feedforward inhibitory responses are even faster than illustrated in Fig. 7. First, as inferred from the analysis of monosynaptic inhibition (see Fig. 3*B*, Table 1B), onsets of g_{GABA_A} could be detected before the corresponding IPSPs. Second, the interneurons used in the dual recordings shown in Fig. 7 represent a selection of non-spontaneously firing cells (with a higher V_{rest} and thus somewhat longer latencies to synaptic spikes). Third, onsets of feedforward IPSPs (Fig. 7) were calculated by substituting

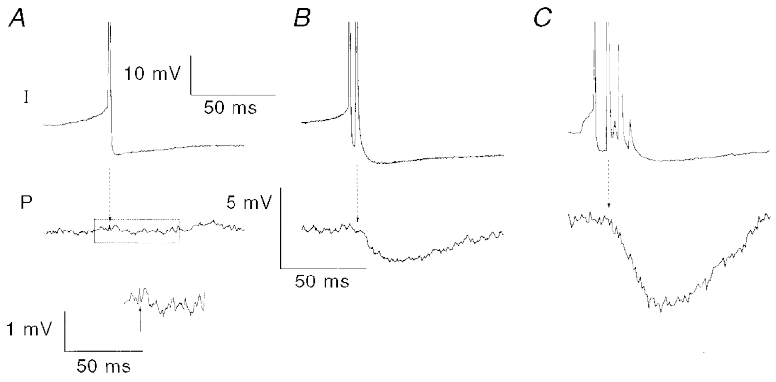

Figure 13. Properties of monosynaptic IPSPs in a weakly coupled pyramidal cell

IPSPs in the pyramidal cell shown in Figs 11 and 12 (also pair 3 in Table 2) were prominent in response to interneuron double (*B*) or triple spikes (*C*), but not in response to single spikes (*A*) (see inset). IPSPs in response to single spikes were revealed upon averaging of several traces (see Fig. 11*Ac*). Onsets of monosynaptic IPSPs in response to multiple presynaptic interneuron spikes were apparently triggered by the second spike as indicated in *C* and *D* (average latency was 2·4 ± 0·4 ms, $n = 22$; in comparison, latency to onset of the averaged IPSP in response to single interneuron APs was 2·3 ms, see Fig. 11*Ac*). IPSP amplitudes were on average 1·9 ± 0·5 mV (following double spikes in *B*) and 5·2 ± 0·9 mV (following triple spikes in *C*).

a 1 ms latency for the onset of the unitary dendritic IPSP. However, latencies to onsets of unitary IPSP could be as short as 0·2 ms (Fig. 6*D*). Therefore – by taking variability of onsets into account – fast onsets of feedforward IPSPs could precede those shown in Fig. 7 by 0·8 ms. Using 0·2 ms instead of 1 ms as latency to unitary IPSP (shown in Fig. 8*A*, see arrows at 300 and 500 μA), complete temporal overlap with the orthodromic pyramidal cell EPSP was observed.

The high degree of temporal overlap between feedforward inhibition and orthodromic excitation (Figs 7 and 8*A*) is a consequence of considerably shorter latencies of interneuron APs (Fig. 12*D*) (Ashwood *et al.* 1984). Steeper EPSP slopes of the interneuron at a given intensity (Table 3A) indicate that the differences in activation kinetics and excitability in the two cell types were linked. Cellular properties of interneurons such as higher input resistance (Table 3A) or different AMPA receptor subunit expression (McBain & Dingledine, 1993; Jonas *et al.* 1994) could be responsible.

Recurrent inhibition

Results show that recurrent inhibitory responses have no impact on the rising phase and peak of the orthodromic EPSP in CA1 pyramidal cells: earliest onsets of recurrent IPSPs occur several milliseconds after the EPSP peak (Table 1B; Fig. 11*B*). Moreover, orthodromic activation of the recurrent inhibitory pathway is the exception. First, elicitation of orthodromic APs in pyramidal cells occurs in general only at very high stimulation intensities (Fig. 8). In addition, orthodromic activation of recurrent inhibition is most probably confined to interneurons that are not connected in a feedforward fashion. In interneurons that are connected in a feedforward manner, the AHP of the synaptic AP prevents recurrent unitary APs (Fig. 12*Da*). The second of synaptic double spikes is more likely to be generated by feedforward excitation (cf. Fig. 8*A* at 700 μA, and Fig. 12*Db*).

The importance of recurrent inhibition in CA1 may lie – in analogy to the CA3 region (Miles & Wong, 1986, 1987) – in containing recurrent excitation (Deuchars & Thomson, 1996; Ali *et al.* 1998). The average latencies of recurrent IPSPs (8·3 ms) in the dual recording (Figs 11–13) were somewhat longer than described for disynaptic recurrent IPSPs in CA3 (Miles, 1990*a*) and CA1 (Sik *et al.* 1995). Possible reasons are as follows. First, interneuron V_{rest} was somewhat higher than average due to the interneuron selection criteria of lack of spontaneous firing. Second, the value of the onset of the unitary IPSP (about 2 ms) was longer due to weak inhibitory coupling (see Table 2). Third, recurrent activation kinetics of bistratified cells could have been slower in comparison with basket cells (Ali *et al.* 1998).

A suprising observation in the mutually coupled pair of cells shown in Figs 11–13 was the occurrence of delayed unitary APs riding on plateau EPSPs in interneurons (Fig. 12). The combination of the slow and fast unitary interneuron APs (Fig. 12*C*) – even faster values have been reported (Miles, 1990*a*; Sik *et al.* 1995) – generated a wide range of latencies (Figs 11*B* and 12*C*). This could be a mechanism in the observed long-lasting presence of $GABA_A$-mediated synaptic influences following afferent stimulation (see Fig. 1*Aa*). The prolonged presence of inhibition conceivably enhances the efficacy of containing recurrent excitation. However, delayed unitary interneuron APs were obtained in a single pair of cells and the general occurrence of this phenomenon remains to be established.

Inhibitory conductances

Although IPSP/IPSCs and g_{GABA_A} were evoked by the same stimulus (Figs 2–4), they may not represent the same event. It was shown in motoneurons that the inhibitory action was considerably faster than indicated by the IPSP (Araki *et al.* 1960). Our kinetic measurements of g_{GABA_A} suggest that $GABA_A$-mediated inhibition may also be considerably faster than indicated by the IPSC (Fig. 3*D*; Table 1). Current measurements were used in previous studies for assessing the effects of inhibitory shunting (Edwards, 1990; Staley & Mody, 1992). While efficacy of shunting can be measured by the time integral of the current waveform, which is subject to much less distortion than the amplitude (Jack *et al.* 1975; Carnevale & Johnston, 1982), measurements of charge transfer to soma do not decrease errors of kinetics that are associated with current measurements. In contrast to IPSP/IPSCs that are derived from spatially diverse sources containing axial and membrane components, inhibitory conductance changes occur in the immediate vicinity of the synapse (Araki *et al.* 1960; Andersen *et al.* 1980; Koch *et al.* 1983).

Based on the temporal interaction of EPSCs and IPSCs, it could have been concluded that synaptic inhibition may primarily affect later parts of the orthodromic EPSP/EPSC such as the delayed NMDA component (Staley & Mody, 1992). Based on the kinetics of g_{GABA_A} (Table 1; Fig. 4), however, it can be concluded – at least in CA1 – that the orthodromic EPSP/EPSC rising phase is tightly controlled by $GABA_A$-mediated inhibition.

How will activity-dependent modification of inhibition change the orthodromic EPSP/EPSC?

A consequence of the shown complete temporal overlap of afferent excitation and inhibition in CA1 pyramidal cells (Figs 4 and 8) is that any modification of $GABA_A$-mediated inhibition will affect the slope and peak of the EPSP. In CA1, the net effect of LTP-inducing tetanization on synaptic inhibition is an EPSP potentiation due to long-term disinhibition caused by impairment of $GABA_A$ receptor function. The evidence is as follows. First, barring effects on GABA release mechanisms, the main action of tetanization on monosynaptic inhibition is impairment of $GABA_A$ receptor function (Stelzer *et al.* 1994). More importantly, a long-term reduction of monosynaptic inhibitory responses by tetanization was demonstrated (Stelzer *et al.* 1994). Second, impairment of $GABA_A$ receptor function is also the main modification of the efficacy of feedforward inhibitory

responses. At the stimulation intensities that are typically used for controls in LTP studies (e.g. 50 % of pyramidal cell EPSP amplitudes, arguably higher in field potential studies), feedforward inhibitory responses are close to their upper limit (see Fig. 8*A* and *B*). The maximal expression of feedforward inhibition during control occludes a potential tetanization-induced increase of interneuron excitability. An enhancement of recurrent inhibition caused by pyramidal cell LTP has no impact on the pyramidal cell EPSP rising phase or peak due to lack of temporal overlap (Fig. 11*B*). In summary, the presented data of temporal interaction of afferent excitation and inhibition in CA1 pyramidal cells support the previous postulate of disinhibition as LTP mechanism (Stelzer *et al.* 1994; Wang & Stelzer, 1996).

Alger, B. E. & Nicoll, R. A. (1982). Feedforward dendritic inhibition in rat hippocampal pyramidal cells studied *in vitro*. *Journal of Physiology* **328**, 105–123.

Ali, A. B., Deuchars, J., Pawelzik, H. & Thomson, A. M. (1998). CA1 pyramidal to basket and bistratified cell EPSPs: dual intracellular recordings in rat hippocampal slices. *Journal of Physiology* **597**, 201–217.

Andersen, P., Dingledine, R., Gjerstad, L., Langmoen, I. A. & Mosfeldt Laursen, A. (1980). Two different responses of hippocampal pyramidal cells to application of γ-aminobutyric acid. *Journal of Physiology* **305**, 279–296.

Andersen, P., Eccles, J. C. & Loyning, Y. (1963). Recurrent inhibition in the hippocampus with identification of the inhibitory cell and its synapses. *Nature* **198**, 540–542.

Andersen, P., Eccles, J. C. & Loyning, Y. (1964). Pathway of postsynaptic inhibition in the hippocampus. *Journal of Neurophysiology* **27**, 608–619.

Araki, T., Eccles, J. C. & Ito, M. (1960). Correlation of the inhibitory postsynaptic potential of motoneurones with the latency and time course of inhibition of monosynaptic reflexes. *Journal of Physiology* **154**, 354–377.

Ashwood, T. J., Lancaster, B. & Wheal, H. V. (1984). *In vivo* and *in vitro* studies on putative interneurons in the rat hippocampus: possible mediators of feedforward inhibition. *Brain Research* **293**, 279–291.

Blanton, M. G., Lo Turco, J. L. & Kriegstein, A. R. (1989). Whole-cell recording from neurons in slices of reptilian and mammalian cortex. *Journal of Neuroscience Methods* **30**, 203–210.

Blasco-Ibanez, J. M. & Freund, T. F. (1995). Synaptic input of horizontal interneurons in stratum oriens of the hippocampal CA1 subfield: structural basis of feedback activation. *European Journal of Neuroscience* **7**, 2170–2180.

Buhl, E. H., Halasy, K. & Somogyi, P. (1994*a*). Diverse sources of hippocampal unitary inhibitory postsynaptic potentials and the number of synaptic release sites. *Nature* **368**, 823–828.

Buhl, E. H., Han, Z. S., Lorinczi, Z., Stezhik, A. S., Karnup, S. V. & Somogyi, P. (1994*b*). Physiological properties of anatomically identified axo-axonic cells in the rat hippocampus. *Journal of Neurophysiology* **71**, 1289–1307.

Buzsaki, G. & Eidelberg, E. (1982). Direct afferent excitation and long-term potentiation of hippocampal. *Journal of Neurophysiology* **48**, 597–607.

Carnevale, N. T. & Johnston, D. (1982). Electrophysiological characterization of remote chemical synapses. *Journal of Neurophysiology* **47**, 606–621.

Davies, C. H., Davies, S. N. & Collingridge, G. L. (1990). Paired-pulsed depression of monosynaptic GABA-mediated inhibitory postsynaptic responses in rat hippocampus. *Journal of Physiology* **424**, 513–531.

Deuchars, J. & Thomson, A. M. (1996). CA1 pyramid–pyramid connections in rat hippocampus *in vitro*: dual intracellular recordings with biocytin filling. *Neuroscience* **74**, 1009–1018.

Edwards, D. H. (1990). Mechanisms of depolarizing inhibition at the crayfish giant motor synapse. I. Electrophysiology. *Journal of Neurophysiology* **64**, 532–540.

Jack, J. J. B., Noble, D. & Tsien, R. W. (1975). *Electric Current Flow in Excitable Cells*. Oxford University Press, London.

Jonas, P., Racca, C., Sakmann, B., Seeburg, P. H. & Monyer, H. (1994). Differences in Ca^{2+} permeability of AMPA-type glutamate receptor channels in neocortical neurons caused by differential GluR-B subunit expression. *Neuron* **12**, 1281–1289.

Kandel, E. R., Spencer, W. A. & Brinley, F. J. (1961). Electrophysiology of hippocampal neurons. I. Sequential invasion and synaptic organization. *Journal of Neurophysiology* **24**, 225–242.

Knowles, W. D. & Schwartzkroin, P. A. (1981). Axonal ramifications of hippocampal CA1 pyramidal cells. *Journal of Neuroscience* **1**, 1236–1241.

Koch, C. (1985). Understanding the intrinsic circuitry of the cat's lateral geniculate nucleus: electrical properties of the spine-triad arrangement. *Proceedings of the Royal Society of London* B **225**, 365–390.

Koch, C., Poggio, T. & Torre, V. (1983). Non-linear interactions in a dendritic tree: localization, timing, and role in information processing. *Proceedings of the National Academy of Sciences of the USA* **80**, 2799–2802.

Lacaille, J.-C. (1991). Postsynaptic potentials mediated by excitatory and inhibitory amino acids in interneurons of stratum pyramidale of the CA1 region of rat hippocampal slices *in vitro*. *Journal of Neurophysiology* **66**, 1441–1454.

Lacaille, J.-C. & Schwartzkroin, P. A. (1988). Stratum lacunosum-moleculare interneurons of hippocampal CA1 region. II. Intrasomatic and intradendritic recordings of local circuit synaptic interactions. *Journal of Neuroscience* **8**, 1411–1424.

Ling, D. S. F. & Benardo, L. S. (1998). Synchronous firing of inhibitory interneurons results in saturation of fast $GABA_A$ IPSC magnitude but not saturation of fast inhibitory efficacy in rat neocortical pyramidal cells. *Synapse* **28**, 91–102.

McBain, C. J. & Dingledine, R. (1993). Heterogeneity of synaptic glutamate receptors on CA3 stratum radiatum interneurons of rat hippocampus. *Journal of Physiology* **462**, 373–392.

Maccaferri, G. & McBain, C. J. (1995). Passive propagation of LTD to stratum oriens-alveus inhibitory neurons modulates the temporoammonic input to the hippocampal CA1 region. *Neuron* **15**, 135–145.

Marty, A. & Neher, E. (1995). Tight-seal whole-cell recording. In *Single-Channel Recording*, ed. Sakmann, B. & Neher, E., pp. 31–52. Plenum Press, New York and London.

Miles, R. (1990*a*). Synaptic excitation of inhibitory cells by single CA3 hippocampal pyramidal cells of the guinea-pig *in vitro*. *Journal of Physiology* **428**, 61–77.

Miles, R. (1990*b*). Variation in strength of inhibitory synapses in the CA3 region of guinea-pig hippocampus *in vitro*. *Journal of Physiology* **431**, 659–676.

Miles, R., Toth, G., Gulyas, A. I., Hajos, N. & Freund, T. (1996). Differences between somatic and dendritic inhibition in the hippocampus. *Neuron* **16**, 815–823.

Miles, R. & Wong, R. K. S. (1986). Excitatory synaptic interactions between CA3 neurones in the guinea-pig hippocampus. *Journal of Physiology* **373**, 397–418.

Miles, R. & Wong, R. K. S. (1987). Inhibitory control of local excitatory synaptic circuits in the guinea-pig hippocampus. *Journal of Physiology* **388**, 611–629.

Pananceau, M., Chen, H. X. & Gustafsson, B. (1997). Long-term potentiation by single volley activation: a mechanism for bicuculline-induced enhancement of synaptic field potentials in the CA1 hippocampal region. *Neuroscience* **79**, 95–101.

Pearce, R. A. (1993). Physiological evidence for two distinct $GABA_A$ responses in rat hippocampus. *Neuron* **10**, 189–200.

Quardouz, M. & Lacaille, J.-C. (1995). Mechanisms of selective long-term potentiation of EPSCs in interneurons of stratum oriens in rat hippocampal slices. *Journal of Neurophysiology* **73**, 810–819.

Sayer, R. J., Redman, S. J. & Andersen, P. (1989). Amplitude fluctuations in small EPSPs recorded from CA1 pyramidal cells in the guinea-pig hippocampal slice. *Journal of Neuroscience* **9**, 840–840.

Scharfman, H. E. (1991). Dentate hilar cells with dendrites in the molecular layer have lower thresholds for synaptic activation by perforant path than granule cells. *Journal of Neuroscience* **11**, 1660–1673.

Schwartzkroin, P. A. (1975). Characteristics of CA1 neurons recorded intracellularly in the hippocampal *in vitro* slice preparation. *Brain Research* **85**, 423–436.

Schwartzkroin, P. A. & Mathers, L. (1978). Physiological and morphological identification of a non-pyramidal hippocampal cell type. *Brain Research* **157**, 1–10.

Sik, A., Penttonen, M., Ylinen, A. & Buzsaki, G. (1995). Hippocampal CA1 interneurons: an *in vivo* intracellular labeling study. *Journal of Neuroscience* **15**, 6651–6665.

Somogyi, P. & Takagi, H. (1982). A note on the use of picric acid-paraformaldehyde fixative for correlated light and electron microscopic immunocytochemistry. *Neuroscience* **7**, 1779–1783.

Staley, K. J. & Mody, I. (1992). Shunting of excitatory input to dentate gyrus granule cells by a depolarizing $GABA_A$ receptor-mediated postsynaptic conductance. *Journal of Neurophysiology* **68**, 197–212.

Stelzer, A., Simon, G., Kovacs, G. & Rai, R. (1994). Synaptic disinhibition during maintenance of long-term potentiation in the CA1 hippocampal subfield. *Proceedings of the National Academy of Sciences of the USA* **91**, 3058–3062.

Taube, J. S. & Schwartzkroin, P. A. (1987). Intracellular recording from hippocampal interneurons before and after development of long-term potentiation. *Brain Research* **419**, 32–38.

Turner, D. A. (1988). Waveform and amplitude characteristics of evoked responses to dendritic stimulation of CA1 guinea-pig pyramidal cells. *Journal of Physiology* **395**, 419–439.

Wang, J.-H. & Stelzer, A. (1996). Shared calcium signaling pathways in the induction of long-term potentiation and synaptic disinhibition in CA1 pyramidal cells. *Journal of Neurophysiology* **75**, 1687–1702.

Wigström, H. & Gustafsson, B. (1983). Facilitated induction of hippocampal long-lasting potentiation during blockade of inhibition. *Nature* **301**, 603–604.

Wong, R. K. S., Prince, D. A. & Basbaum, A. I. (1979). Intradendritic recordings from hippocampal neurons. *Proceedings of the National Academy of Sciences of the USA* **76**, 986–990.

Yamamoto, C. (1972). Intracellular study of seizure-like afterdischarges elicited in thin hippocampal sections *in vitro*. *Experimental Neurology* **35**, 154–164.

Acknowledgements

These studies were supported by the NIH (NS30144-01). We thank Dr R. Bianchi and Dr D. Ling for critically reading the manuscript.

Corresponding author

A. Stelzer: Department of Physiology and Pharmacology, Box 29, State University of New York, 450 Clarkson Avenue, Brooklyn, NY 11203, USA.

Email: astelzer@netmail.hscbklyn.edu

Author's permanent address

S. Karnup: Institute of Theoretical and Experimental Biophysics, 142292 Puschino, Russia.